published by Ural Federal University
eISSN 2411-1414
chimicatechnoacta.ru

REVIEW
2025, vol. 12(2), No. 12214
DOI: 10.15826/chimtech.2025.12.2.14

Adsorption isotherms, thermodynamics, and kinetics of activated carbon as adsorbent to water pollutants: a review

Muhamad Jalil Baari [a] *, La Rudi [b], La Harimu [b]

a: Department of Chemistry, Faculty of Science and Technology, Universitas Sembilanbelas November Kolaka, Kolaka 93517, Indonesia
b: Department of Chemistry Education, Faculty of Teacher Training and Education, Universitas Halu Oleo, Kendari 93132, Indonesia
* Corresponding author: jalilbaari@gmail.com

Abstract

Water pollutants, such as dyes and heavy metals, which cause various health and environmental problems, challenge researchers to investigate activated carbon-based adsorbents. These adsorbents are obtained from natural sources or waste, so they are environmentally friendly. The literature reveals that the adsorption capacities of activated carbons obtained from experiments, isotherm equations, and kinetic equations are relatively high but vary in value. The abundance of functional groups as active sites and the spread of pores or cavities on the adsorbent surface affect the efficiency of adsorption. This review aims to overview the adsorption isotherms, thermodynamic properties, and kinetic behaviors of several activated carbons from natural sources and waste. The maximum adsorption capacity of the dyes is in the range of 2.0–1169.25 $mg \cdot g^{-1}$, while the maximum adsorption capacity of heavy metals is in the range of 0.488–312.5 $mg \cdot g^{-1}$. The different adsorption mechanisms, the convenience of adsorption, adsorption energy, the spontaneity of adsorption, and the rate-determining step are described for each type of activated carbon. Therefore, specified information about their performances toward different water pollutants can be evaluated. Moreover, potential improvements in the performance of existing adsorbents can be gained through further research based on the findings of this review.

Key findings

- Various activated carbons from natural sources and waste as water pollutant adsorbents with different activation methods reported in 2017–2024 are overviewed.
- Morphological structure and performance of activated carbons from natural sources and waste as water pollutant adsorbents are listed.
- Adsorption isotherms, thermodynamic, and kinetic studies of activated carbon-based adsorbents from natural sources and waste are outlined.
- The limitations and proposals for further studies are explained.

Accompanying information

Article history
Received: 10.03.25
Revised: 29.03.25
Accepted: 04.04.25
Available online: 23.04.25

Keywords
Activated carbon; adsorbent; adsorption isotherms; kinetics; thermodynamics; water pollutants

Funding
None.

Supplementary information
Transparent peer review: READ

Sustainable Development Goals
6 CLEAN WATER AND SANITATION

1. Introduction

Water pollution is a big problem in the life of aquatic organisms and the water environment. The presence of pollutants inflicts various diseases or nuisances on humans, animals, and plants [1,2]. In addition, the water pollutants also reduce environmental hygiene and the aesthetic quality of water [3,4]. Most of the pollutants originate from dyes and heavy metals. Current methods to overcome water pollutants consist of coagulation, membrane processes, enzymatic decomposition, ion exchange, photodegradation, liquid membrane transport, chemical oxidation, and adsorption [5–9]. The adsorption method is an effective and efficient way of wastewater treatment. It is easy to operate, well-designed, relatively low-cost, and resistant to toxic pollutants [10]. Theoretically, adsorption involves the transfer of specified material from the liquid phase to a solid surface. It is initiated by van der Waals, ionic, and metallic interactions. Additionally, chemical bonds can form when there is sufficient energy. The products of the adsorption process are usually not dangerous substances [11].

A substance capable of adsorbing other substances is referred to as an adsorbent. Several organic or natural materials have been identified as adsorbents for heavy metals, dyes, and other pollutants in wastewater or aqueous solutions. The elections of adsorbent materials for removing water pollutants should consider availability, renewability, adsorption capability and capacity, biodegradability, hydrophilicity, and chemical or mechanical resistance. An example of an adsorbent used for pollutant adsorption is activated carbon. Activated carbons can be made from various natural substances that are rich in carbon sources by way of carbonizing, activation, and other processing steps [12]. The activation process consists of physical or chemical ways that intend to increase the adsorption capacity of a material [13]. Physical activation refers to eliminating volatile substances from carbon material through high-temperature treatment. After that, the material is automatically activated by activating agents, for instance, steam, CO_2, air, or a combination of them [14]. On the other side, chemical activation involves the addition of chemical reagents from inorganic compounds like KOH, H_2SO_4, NaOH, H_3PO4, $ZnCl_2$, etc. Each activation method has its own advantages. Physical activation does not need chemical reagents, so it is more environmentally friendly [15]. On the other hand, chemical activation occurs at low temperatures (resulting in lower energy consumption), requires a shorter processing time, and produces a large surface area with well-developed microporosity [16,17]. Different sources of adsorbents, activation techniques, and synthesizing methods will produce different characteristics of the activated carbons [13]. The superiorities of activated carbon utilization in wastewater treatment are observed by thermal stability, mechanical strength, high porosity, and high surface area [18].

Studies into water pollutant adsorption determine adsorption efficiency and adsorption capacity of the adsorbents in various conditions. The optimum performance of the adsorbent is measured by varying adsorbent and pollutant concentrations, system temperatures, pH values, and contact times. Recent studies have investigated adsorption isotherm, thermodynamic, and kinetic parameters to obtain the adsorption mechanism of adsorbate on the adsorbent, adsorption energy, and order kinetic model, respectively. Other parameters like constants related to adsorption properties of activated carbons and validation methods can be obtained from those investigations. A review of dye removal using adsorbents was conducted [2, 19]. The types of adsorbents, adsorbates, and factors that affect the adsorption process were reported. Then, the use of activated carbon, microorganisms, and nanomaterials to adsorb heavy metals were also reviewed [20–22]. These reviews explain the parameters that influence the performance of adsorbents. Meanwhile, specific studies into adsorption isotherm, thermodynamic, and kinetic parameters concerning activated carbons from natural sources and waste as water pollutant adsorbents, especially dyes and heavy metals, have not been reviewed. Natural sources are chosen due to because they contain compounds with active functional groups, biodegradability, bioavailability, regeneration ability, reusability, and porous structures. Therefore, this review focuses on discussing the utilization of activated carbon from various natural sources and wastes as dyes and heavy metal adsorbent in the aqueous phase. A comprehensive understanding of adsorption isotherms, thermodynamic properties, and kinetic behaviors will be discussed to gain insight into the adsorption mechanism, adsorption energy, spontaneity of adsorption, reaction order, rate-determining step, and validation methods of the various activated carbons from natural sources and waste. A literature review was conducted on some recent research articles published in 2017–2024.

1.1. Heavy metals

Elements that are classified as heavy metals consist of copper (Cu), chromium (Cr), lead (Pb), cadmium (Cd), iron (Fe), mercury (Hg), zinc (Zn), nickel (Ni), manganese (Mn), arsenic (As), cobalt (Co), etc. Cu, Fe, Zn, and Mn are included in essential toxic heavy metals, while the others are non-essential toxic heavy metals [23]. These metals have density of more than 4 $g.cm^{-3}$ [24]. Heavy metals spread widely in the environment because metal compounds are used in many fields such as medicines, construction materials, mining, chemicals, electronics, photography, cosmetics, etc. [25–27]. The existence of heavy metals in the environment is a serious problem due to their non-biodegradability, carcinogenicity, toxicity for organisms, and food chain contamination [28, 29]. Water or the marine environment can be contaminated through natural mineral dissolution from seawater movement [30]. This will disrupt the aquatic ecosystem, especially aquatic animals consumed by humans. Long-time exposure to heavy metals in the human body is harmful because of its carcinogenic, teratogenic, toxic, and irritant characteristics [28].

Adsorption is an effective and efficient method to remove heavy metals from water. Several types of materials with adsorption capability are carbon-based, chitosan-based, and mineral (clay, zeolite, and silica) adsorbents [31]. Carbon-based adsorbents are often chosen owing to their porous structures and affinity from the presence of functional groups.

1.2. Dyes

Dyes are chemical substances for coloring products. Those are widely used in many fields such as textile, printing, rubber, plastic, etc. [32–34]. The high demand for product colorization makes synthetic dyes more widely used. Two principal components on dye substance are chromophore and auxochrome. Chromophore is responsible for creating the color, whereas auxochrome increases the affinity of dye toward fibers [35]. The synthetic dyes consist of ionic (reactive, acid, and direct dyes) and non-ionic (vat and disperse dyes) dyes [36]. Ionic dyes are classified into cationic and anionic dyes. Cationic dyes encompass methylene blue (MB), nile blue (NB), brilliant green (BG), and methyl violet (MV) [37]. Anionic dyes comprise methyl

DOI: 10.15826/chimtech.2025.12.2.14

orange (MO), eriochrome black T (EBT), Congo red (CR), Reactive Blue 19 (RB19), Sumifix Supra Brilliant Red 3BF (RR195), Naphthol blue black (NBB), and methyl red (MR) [38].

Based on their chemical structure, dyes are classified into azo, triarylmethane, nitro, indigoid, nitroso, and anthraquinone groups [39]. Dye waste is always produced as a side product during the production process [40]. Despite undergoing treatment processes, this substance remains present in water discharges. Dye pollutants have complex molecular structures, which makes them difficult to biodegrade [41]. The presence of dyes in wastewater causes many problems; for instance, a decrease in dissolved oxygen concentration induces respiratory problems, inhibits the plants' photosynthesis, is toxic/carcinogenic for humans and microorganisms, and is aesthetically unpleasant [4, 10]. Direct inhalation of several dyes inflicts breathing difficulty and indigestion problems [42]. The utilization of activated carbon from various sources has been proven effective in reducing the content of various synthetic dyes in wastewater [43]. It is an inexpensive precursor material and can be reused multiple times.

2. Carbon sources and activated carbon

Natural or organic substances are generally processed to obtain activated carbons (AC) because all plants contain carbon elements in various forms, like carbohydrates, proteins, and lipids. Activated carbon produced from expired beverages utilizes the sugar content, including sucrose, fructose, and glucose. On the other hand, activated carbons were obtained from dragon fruit peels after being converted from lignocellulosic biomass. Sunflower pith and coconut shell contain holocellulose as the primary carbon source [44]. Winemaking wastes (Bagasse and cluster stalks) were converted to hydrothermal carbon before being chemically activated and carbonized, forming AC. Meanwhile, the fiber of peanut shells contains cellulose, lignin, and hemicellulose [45]. The general synthesis scheme of activated carbon from various natural sources is displayed in Figure 1. Afterward, notable stages related to the use of those activated carbons covered in this review are shown in Figure 2.

The activation method contributes to creating and widening pore sizes [46, 47]. An example is activation temperature, also known as physical activation. The increase in activation temperature from 500 °C to 800 °C can break the bonds of complex molecules that were contained in lignocellulosic biomass to open as well as enlarge micropores and mesopores of the activated carbon [48]. Hence, it can decrease the yield of activated carbon. For chemical activation, the activating compound determines % yield and water pollutant adsorption. Physical activation can produce higher yields than chemical activation. This phenomenon was observed in the use of rice straw as activated carbon, where both physical and chemical activation processes were carried out at 700 °C [49]. The dissolution of certain substances during the washing stage and structural degradation caused by the presence of the activating agent may contribute to this outcome. Meanwhile, KOH activation produces more % yield than NaOH activation due to higher reactivity toward lignocellulose [50].

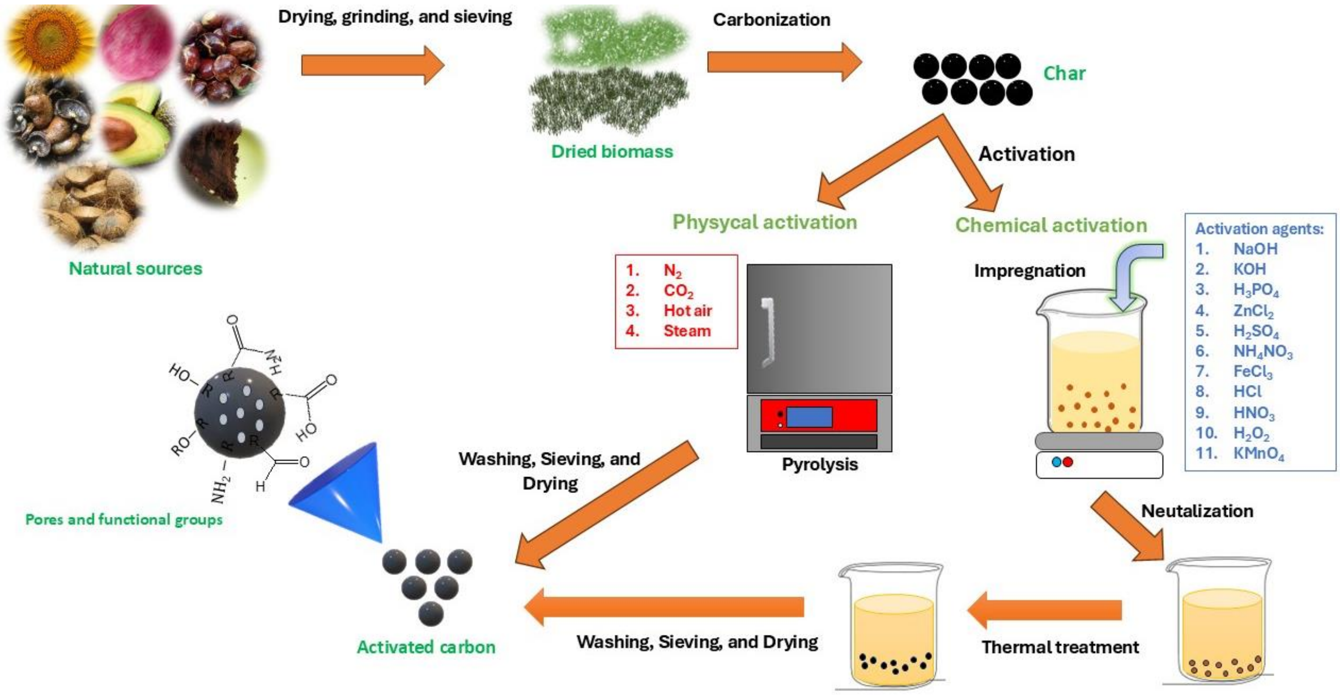

Figure 1 Synthesis scheme of activated carbon from natural sources/biomass.

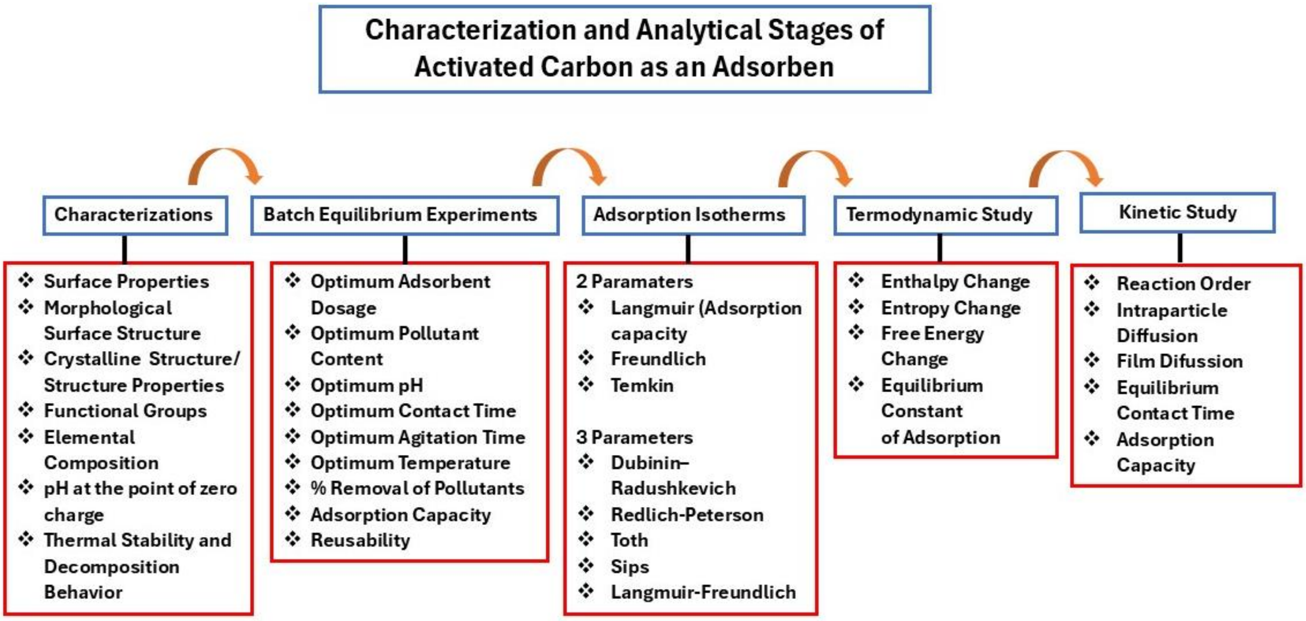

Figure 2 Notable stages concerning the use of activated carbon-based adsorbents from natural sources.

Pre-carbonization process before KOH activation enhances the AC yield and its surface area [51]. Meanwhile, activation by H_3PO_4 generates higher yields than KOH activation owing to easier decomposition with respect to breaking of chemical bonds on the biopolymer [49]. NaOH and $ZnCl_2$ activation can initiate the formation of new micropores on the activated carbon, whereas KOH activation improves micropore volume on the AC greater than NaOH activation [52,53]. Meanwhile, using phosphoric acid as an activator induces the formation of mesopores rather than micropores [54]. The synergetic effect of the mesopore and micropore is influential since the diameter of dye molecules is well-defined. The internal diffusion stage mostly occurs on mesopores, while micropores act to increase surface energy through irreversible adsorption [55,56]. AC based on date pits that is NaOH-activated, adsorbs methylene blue better than that after KOH activation [48]. Additional treatment by ultrasound assistance generates more pores and cavities after breaking the bonds that connect functional groups [57]. Adsorption capacity slightly increases compared to physical and general chemical activation. NaOH activation to make activated carbon from peanut shells also results in a higher adsorption capacity toward MB than $ZnCl_2$ and steam activations. In other studies, KOH activation was used to create new pores and expand the existing pores [58]. Meanwhile, the amount of pollutant adsorbed per gram of AC or adsorption capacity, q_e (mg·g⁻¹) is calculated by Equation 1 [59]:

$$q_e = \frac{(C_0 - C_e)V}{m}, \tag{1}$$

where C_o is the initial concentration of pollutant (mg·L⁻¹) in the testing solution, C_e is the pollutant concentration in equilibrium (mg·L⁻¹), V is the volume of pollutant solution (L), and m is the mass of the AC used in the experiment.

Most reports of the surface area generally use the Brunauer–Emmett–Teller technique. However, the Dubinin-Radushkevich equation used to calculate the surface area of an adsorbent with a pore size far from 0.9 nm is advisable [60]. Tables 1 and 2 summarize the activated carbons, adsorption capacities, and morphologies obtained from natural sources for dyes and heavy metals, respectively. In addition, complete information for the application of activated carbons from waste as adsorbents is listed in Table 3.

The ability of activated carbon to adsorb water pollutants is diverse. Nutmeg shell-activated carbon is preferable for adsorbing Pb(II) ions rather than Cu(II) ions. This is due to the nature of Pb, which is more electronegative than Cu, so that Pb(II) ions will be more easily adsorbed on the adsorbent surface [98]. Then, the experimental adsorption capacity of prickly pear seed cake is higher for MB adsorption than for MO in similar conditions.

pH value and contact time in the adsorption processes affect the adsorbent capability to attract adsorbates. An increase in pH up to 10 can escalate cationic dye removal. Negative charges on the surface of activated carbon are formed when the solution pH is close to 10. Thus, electrostatic interactions with cationic dyes are enhanced. Functional group types on the activated carbon have an important role in this condition. Activated carbons from coconut shells, date pits, rice straw, dragon fruit, bamboo chips, coffee husk, and peanut shell are effective for methylene blue at pH>7. On the contrary, activated carbon with positive charges on its surface prefers to adsorb anionic dyes at lower pH (pH≈7 or lower).

Table 1 Several natural sources of activated carbon, types of dye pollutants, experimental adsorption capacities, surface area, pore size, and pore volume of adsorbent.

No.	Source of activated carbon and activation method	Dye Pollutant	Maximum adsorption capacity (mg·g^{-1})	Surface area (m^2·g^{-1}) Equation	Pore size (nm) and pore volume (cm^3·g^{-1})	Ref.
1	Date pits (CA by NaOH and KOH)	Methylene blue	NaOH: 149.25 (50 °C, pH 9) KOH: 99.77	NaOH: 377.63	NaOH: 2.117 nm 0.028 cm^3·g^{-1}	[48]
2	Karanj fruit hulls (CA by KOH)	Methylene blue	239.4 (50 °C)	828.30 BET 1145.84 Langmuir	1.992 nm 0.36 cm^3·g^{-1}	[58]
3	Winemaking waste: Bagasse (CA by KOH)	Methylene blue	1156.65 (dosage: 10 mg/50 mL, 80 °C, contact time: 3 h)	1337 Dubinin–Radushkevich 1861 BET	1.19 nm 0.82 cm^3·g^{-1}	[59]
4	Winemaking waste: Cluster stalks (CA by KOH)	Methylene blue	1169.25 (dosage: 10 mg/50 mL, 80 °C, contact time: 3 h)	1194 Dubinin–Radushkevich 2262 BET	1.71 nm 1.4 cm^3·g^{-1}	[59]
5	Sunflower piths (CA by NaOH and KOH)	Methylene blue	NaOH: 965 KOH: 580	NaOH: 2690 KOH: 2090 BET	NaOH: 2.6 nm 1.75 cm^3·g^{-1} KOH: 2.37 nm 1.24 cm^3·g^{-1}	[50]
6	Rice straw (PA by N_2 and CO_2; CA by KOH and H_3PO_4)	Methylene blue	N_2: 105.1 CO_2: 44.2 KOH: 527.6 H_3PO_4: 209.1	N_2: 158.1 CO_2: 214.7 KOH: 1973 H_3PO_4: 629.1 BET	N_2: 0.129 cm^3·g^{-1} CO_2: 0.164 cm^3·g^{-1} KOH: 1.131 cm^3·g^{-1} H_3PO_4: 0.935 cm^3·g^{-1}	[49]
7	Rice straw (PA by N_2 and CO_2; CA by KOH and H_3PO_4)	Congo red	N_2: 245.1 CO_2: 253.9 KOH: 531.4 H_3PO_4: 208.4	N_2: 158.1 CO_2: 214.7 KOH: 1973 H_3PO_4: 629.1	N_2: 0.129 cm^3.g^{-1} CO_2: 0.164 cm^3.g^{-1} KOH: 1.131 cm^3.g^{-1} H_3PO_4: 0.935 cm^3.g^{-1}	[49]
8	Liquefied wood (CA by $ZnCl_2$)	Methylene blue	725.63 (MB conc.: 600 mg·L^{-1}, 5 h)	1086	1.5–2 nm 0.953 cm^3·g^{-1}	[53]
9	Coconut Shell (PA by hot air and CA by H_3PO_4)	Methylene blue	PA: 6.74 (pH 8, contact time: 60 min) CA: 6.10 (pH 8, contact time: 40 min)	–	–	[61]
10	Rice straw (CA by KOH)	Methylene blue	300 mol·g^{-1} (adsorbent dosage: 1 g/300 mL MB concentration, MB conc.: 4 mg·L^{-1}, pH 10, 293 K)	–	45–55 μm	[62]
11	Dragon fruit peels (CA by KOH)	Methylene blue	175 (adsorbent dosage: 0.8 g·L^{-1}, pH 10, 50 °C, MB conc.: 200 mg·L^{-1})	756.3 BET	11.3 nm 0.376 cm^3·g^{-1}	[63]
12	Bamboo chip (CA by KOH)	Methylene blue	105.87 (adsorbent dosage: 0.1 g, pH 10, 40 °C, MB conc.: 100 mg·L^{-1})	720.69 BET	7.32 nm 0.368 cm^3·g^{-1}	[64]
13	Prickly pear seed cake (CA by H_3PO_4)	Methyl orange	194.08 (20 °C and pH 7)	–	–	[65]
14	Prickly pear seed cake (CA by H_3PO_4)	Methylene blue	260 (20 °C and pH 7)	–	–	[66]
15	Sugar scum powder (PA by hot air)	Methyl orange	5.32 (adsorbent dosage: 16 g·L^{-1}, 22 °C and pH 7.2, MO conc.: 100 mg·L–1)	–	–	[67]
16	Rice husk (CA by H_2SO_4 and H_3PO_4)	Sumifix Supra Brilliant Red 3BF (RR195)	2.0 (adsorbent dosage: 13 g·L^{-1}, pH 2, agitation speed: 100 rpm)	–	–	[68]
17	Eucalyptus wood chips (PA by steam)	Methylene blue	96.93	870.473 BET	0.215 cm^3·g^{-1}	[69]
18	Spent coffee grounds (CA by KOH)	Aniline yellow	2.58 (adsorbent dosage: 0.6 g, AY conc.: 35 ppm, contact time: 2.5 h)	–	–	[70]
19	Seed hair fibers of	Methylene blue	685.25 (adsorbent dosage: 50	1779.003	3.106 nm	[71]

DOI: 10.15826/chimtech.2025.12.2.14

No.	Source of activated carbon and activation method	Dye Pollutant	Maximum adsorption capacity ($mg\cdot g^{-1}$)	Surface area ($m^2\cdot g^{-1}$) Equation	Pore size (nm) and pore volume ($cm^3\cdot g^{-1}$)	Ref.
	metaplexis japonica (CA by H_3PO_4)		mg, MB conc.: 360 $mg\cdot L^{-1}$, 25 °C, 120 rpm)		1.613 $cm^3\cdot g^{-1}$	
20	Camellia oleifera seed shell (CA by KOH)	Methylene blue	462.67 (adsorbent dosage: 0.5 g, pH 4 and 8, MB conc.: 200 $mg\cdot L^{-1}$)	1882.41 BET	2.168 nm 0.072 $cm^3\cdot g^{-1}$	[72]
21	Peanut shell (CA by NaOH and $ZnCl_2$; PA by steam)	Methylene blue	NaOH: 350 (pH 12, 50 °C, MB Conc.: 150 ppm, contact time: 90 minutes, adsorbent dosage: 0.4 $g\cdot L^{-1}$) $ZnCl_2$: 50 (pH 12, 50 °C, MB Conc.: 325 ppm, contact time: 45 min, adsorbent dosage: 0.04 $g\cdot L^{-1}$) Steam: 150 (pH 10, 50 °C, MB Conc.: 275 ppm, contact time: 90 min, adsorbent dosage: 0.4 $g\cdot L^{-1}$)	Not written clearly BET	4–5 nm	[73]
22	Cashew nut shell (CA by KOH)	Brilliant green	99 (BG conc.: 50 $mg\cdot L^{-1}$, adsorbent dosage: 0.1 $g\cdot L^{-1}$, pH 6, contact time: 90 min)	407.8 BET	2–15 nm 0.29 $cm^3\cdot g^{-1}$	[74]
23	Coffee husk from Coffee arabica (CA by H_2SO_4)	Methylene blue	19.988 (MB conc.: 100 mg·L–1, adsorbent dosage: 4.83 $g\cdot L^{-1}$, pH 8.12, contact time: 60 min)	0.9853 BET	–	[75]
24	Dodonaea Viscosa (DV) into beads of calcium-alginate (ACAB) (CA by $ZnCl_2$)	Methylene blue	DV: 239 ACAB: 370 (MB conc.: 50 $mg\cdot L^{-1}$, adsorbent dosage: 250 mg, 77 °C, pH 8, contact time: 70 min)	–	–	[76]
25	Oak Cupules (CA by H_3PO_4)	Naphthol blue black and crystal violet	NBB: 208 (adsorbent dosage: 0.08 g, NBB conc.: 50 $mg\cdot L^{-1}$, pH 2, contact time: 180 min) CV: 658 (adsorbent dosage: 0.04 g, CV conc.: 50 $mg\cdot L^{-1}$, pH 12, contact time: 90 min)	–	–	[77]

Notes: No. 22: Maximum adsorption capacity is written as maximum removal efficiency (%).

Table 2 Several natural sources of activated carbon, types of heavy metal pollutants, experimental adsorption capacities, surface area, pore size, and pore volume of adsorbent.

No.	Source /type of activated carbon	Heavy metal pollutant	Maximum adsorption capacity ($mg\cdot g^{-1}$)	Surface area ($m^2\cdot g^{-1}$) Equation	pore size (nm) and pore volume ($cm^3\cdot g^{-1}$)	Ref.
1	Jengkol (*Pithecellobium Jiringa* shell) (CA by NaOH with ultrasound assistance)	Cu(II)	104.17 (1.0 g, 30 °C, pH 4.5, Cu(II) conc.: 1190.5 $mg\cdot L^{-1}$)	–	–	[57]
2	Banana Peel (CA by KOH)	Cu(II), Ni(II), and Pb(II)	Cu(II): 14.3 (2.4 $g\cdot L^{-1}$, pH 6.5) Ni(II): 27.4 (1.8 $g\cdot L^{-1}$, pH 6.4) Pb(II): 34.5 (0.9 $g\cdot L^{-1}$, pH 6.1)	63.5 BET	2.22 nm 0.014 $cm^3\cdot g^{-1}$	[78]
3	Australian Pine Cones (PA and CA by NaOH consecutively)	Cu(II)	26.71 (340.81 $mg\cdot L^{-1}$, contact time: 2 h, activator ratio: 0.6)	–	–	[79]
4	Apple peel (CA by H_3PO_4)	Cr(VI)	34.59 (Cr(VI) conc.: 50 $mg\cdot L^{-1}$, adsorbent dosage: 0.15 g, 28 °C, pH 2, 400 rpm, contact time: 2 h)	–	–	[80]
5	Bean dreg (PA by steam and heat consecutively)	Cr(VI)	3.3 $mmol.g^{-1}$ (adsorbent dosage: 1 g·L–1, 25 °C, pH 2, contact time: 24 h, Cr(VI) conc.: 8 $mmol\cdot L^{-1}$)	1004 BET	0.5 $cm^3\cdot g^{-1}$	[81]
6	Elm tree (CA by KOH)	Cr(VI) and Pb(II)	Pb(II): 232.56 (pH 5, adsorbent dosage: 0.01 g/25 mL, 250 rpm, contact time: 60 min)	1085 BET	1.764 nm 0.4991 $cm^3\cdot g^{-1}$	[82]

DOI: 10.15826/chimtech.2025.12.2.14

No.	Source /type of activated carbon	Heavy metal pollutant	Maximum adsorption capacity ($mg \cdot g^{-1}$)	Surface area ($m^2 \cdot g^{-1}$) Equation	pore size (nm) and pore volume ($cm^3 \cdot g^{-1}$)	Ref.
			Cr(VI): 113.63 (pH 2, adsorbent dosage: 0.01 g/25 mL, 250 rpm, contact time: 60 minutes)			
7	Pistachio wood (CA by NH_4NO_3 and KOH consecutively)	Pb(II)	190.2 (pH 6, adsorbent dosage: 0.25 $g \cdot L^{-1}$, Pb(II) conc.: 5.5 $mg \cdot L^{-1}$, contact time: 30 min)	1884 BET	2.11 nm 0.994 $cm^3 \cdot g^{-1}$	[52]
8	Carrot, tomato, polyethylene terephthalate composite (CA by $ZnCl_2$ and $FeCl_3$ consecutively)	Co(II)	312.5 (adsorbent dosage: 0.8 $g \cdot L^{-1}$, contact time: 99 min, pH 9.74)	–	–	[83]
9	Camellia oleifera seed shell (CA by KOH)	Cr(VI)	284.6 (adsorbent dosage: 0.25 g, pH 2, Cr(VI) conc.: 150 $mg \cdot L^{-1}$)	1882.41 BET	2.168 nm 0.072 $cm^3 \cdot g^{-1}$	[72]
10	Avocado seed biomass (CA by H_3PO_4)	Cr(VI) and Pb(II)	Cr(VI): 6 (Cr(VI) conc.: 90 $mg \cdot L^{-1}$, pH 5, 25 °C, 200 rpm, adsorbent dosage: 0.5 $g \cdot L^{-1}$) Pb(II): 24 (Pb(II) conc.: 180 $mg \cdot L^{-1}$, pH 5, 25 °C, 200 rpm, adsorbent dosage: 0.2 $mg \cdot L^{-1}$)	0.1276 BET	0.0001 $cm^3 \cdot g^{-1}$	[84]
11	Empty palm oil fruit bunches and carbide waste (PA)	Fe(II)	0.75 (Empty palm oil fruit bunches : carbide waste = 2.5:2, contact time: 2 h, pH 12.75)	–	–	[85]
12	Ziziphus lotus (CA by H_2SO_4)	Cd and Cr(VI)	Cd: 11.070 Cr(VI): 8.938 (adsorbent dosage: 70 $mg \cdot L^{-1}$, Contact time: 80 min)	–	6000 to 50000 nm	[86]
13	Coffee grounds (CA by H_2SO_4)	Cd and Cr(VI)	Cd: 5.92 Cr(VI): 5.767 (adsorbent dosage: 70 $mg \cdot L^{-1}$, Contact time: 80 min, 50 °C)	–	6000 to 50000 nm	[86]
14	Nutmeg shell (CA by H_3PO_4)	Pb(II) and Cu(II)	Pb(II): 0.794 (40 min, pH 5) Cu(II): 0.488 (70 min, pH 4)	19.624	4.823 nm 0.0237 $cm^3 \cdot g^{-1}$	[87]
15	Coconut shell (CA by $ZnCl_2$	Fe(II) and Pb(II)	Fe(II): 9.67 (adsorbent dosage: 1 $g \cdot L^{-1}$, contact time: 4 h, pH 7, 300 rpm, Fe(II) conc.: 35 $mg \cdot L^{-1}$) Pb(II): 10.04 (adsorbent dosage: 1 $g \cdot L^{-1}$, contact time: 4 h, pH 11, 300 rpm, Pb(II) conc.: 35 $mg \cdot L^{-1}$)	–	–	[88]
16	Peanut shell (PA by steam)	Pb(II)	>40 (pH 4.5, Pb(II) conc.: > 175 ppm, contact time: 1.5 h, adsorbent dosage: 2.75 $g \cdot L^{-1}$	–	0.4–0.5 nm	[73]
17	Cypress fruit (CA by H_3PO_4)	Pb(II), Co(II), Cd(II)	Pb(II): 81.87 (pH 7, Adsorbent dosage: 0.06 g, Pb(II) conc.: 50 $mg \cdot L^{-1}$, contact time: 1.5 h) Co(II): 55.3 (pH 6, Adsorbent dosage: 0.04, Co(II) conc.: 70 $mg \cdot L^{-1}$, contact time: 1.5 h) Cd(II): 117.3 (pH 11, Adsorbent dosage: 0.08 g, Cd(II) conc.: 70 $mg \cdot L^{-1}$, contact time: 1.5 h)	–	–	[89]
18	Spent brewery barley husks (CA by H_3PO_4)	Cd(II)	5.0 (pH 6, contact time: 5 min, adsorbent dosage: 0.1 g)	–	–	[90]

DOI: 10.15826/chimtech.2025.12.2.14

Table 3 Several activated carbons from wastes, types of dye pollutants, experimental adsorption capacities, surface area, pore size, and pore volume of adsorbent.

No.	Source /type of activated carbon	Water pollutant	Maximum adsorption capacity (mg·g^{-1})	Surface area (m^2·g^{-1}) Equation	Pore size (nm) and pore volume (cm^3·g^{-1})	Ref.
1	Waste carpets (CA by H_3PO_4)	Methylene blue	769.2 (35 °C, pH 8, adsorbent dosage: 8 g·L^{-1}, contact time: 12 h, MB concentration: 700 mg·L^{-11})	953 BET	1.48 nm 0.694 cm^3·g^{-1}	[91]
2	Activated carbon with Zinc from Electric arc furnace dust	Reactive Blue 19 (RB19) Chromatin Yellow 3247 (CY3247)	48.35 (RB19 conc. 25 mg·L^{-1}, contact time: 30 min, pH 9, 60 °C) 45.91 (CY3247 conc.: 25 mg·L^{-1}, contact time: 30 min, pH 9, 60 °C)	62.5 BET 114.5 Langmuir	<20 nm 0.0398 cm^3·g^{-1}	[92]
3	Denim fabric residue (CA by H_3PO_4)	Pb(II)	Cellulose: 369.82 (Pb(II) conc.: 500 mg·L^{-1}) Cellulose-polyester: 359.77 (Pb(II) conc.: 500 mg·L^{-1})	Cellulose: 1714 Cellulose-polyester: 1743 BET	Cellulose: 3.02 nm; 0.67 cm^3·g^{-1} Cellulose-polyester: 2.80 nm; 0.58 cm^3·g^{-1}	[54]
4	Fe_3O_4-waste paper activated carbon composite (CA by HCl)	Methylene blue	52.34 (adsorbent dosage: 2.5 g·L^{-1}, 318 K, pH 6)	–	–	[93]
5	Activated charcoal (Activation by water)	Acid blue and basic blue	151.3 (adsorbent dosage: 10 mg at 55 °C)	–	–	[94]
6	Expired beverage (CA by KOH)	Methylene blue	413.43 (55 °C)	1273 BET	2.05 nm 0.632 cm^3·g^{-1}	[95]
7	Paper waste (CA by H_2O_2, HNO_3, and $KMnO_4$)	Methylene blue and Cr(VI)	H_2O_2: MB: 30.01 (200 mg·L^{-1}, 60 min, pH 10) Cr(VI): 28.83 (200 mg·L^{-1}, 120 min, pH 2) HNO_3: MB: 34.0 (200 mg·L^{-1}, 60 minutes, pH 10) Cr(VI): 33.46 (200 mg·L^{-1}, 120 min, pH 2) $KMnO_4$: MB: 31.3 (200 mg·L^{-1}, 60 min, pH 10) Cr(VI): 31.06 (200 mg·L^{-1}, 120 min, pH 2)	H_2O_2: 21.9 HNO_3: 34.8 $KMnO_4$: 26.2	H_2O_2: 0.05 cm^3·g^{-1} HNO_3: 0.061 cm^3·g^{-1} $KMnO_4$: 0.047 cm^3·g^{-1}	[96]
8	ZnO-date palm spikelets composites (CA by $ZnCl_2$ and PA consecutively)	Methyl orange	199.6 (MO conc.: 200 mg·L^{-1}, adsorbent dosage: 65 mg, contact time: 240 min, pH 2, 20 °C, NaCl conc.: 0.2 M)	–	6100 nm	[97]

Notes:
CA : Chemical activation;
PA : Physical Activation;
– : Not mentioned.

The effective adsorption at a relatively lower pH generally occurs in the case of heavy metal adsorption. For instance, Cr(VI) adsorption takes place optimally at pH 2 due to its oxyanion forms in the aqueous solution [81]. At the same time, hydrogen ion (H^+) uptake also occurs at lower pH, thereby reducing other heavy metals adsorption [78]. The effect of the functional groups is diminished in the utilization of jengkol AC as a Cu(II) adsorbent. These functional groups are substituted by pores and cavities that serve as active sites. Hence, this material still adsorbs Cu(II) preferably in acid conditions (pH<7). Activated carbon from expired beverages has a pH$_{zpc}$ 6.30. Thus, adsorption capacity does not increase significantly when pH is above 6.30. Different conditions were experienced for AC from Karanj fruit hulls. Its pH$_{zpc}$ is 4.1. The increase in solution pH will deprotonate the active site of the AC to intensify electrostatic interaction with positively charged pollutants.

Meanwhile, the contact time between adsorbent and pollutants must be appropriate because the diffusion process of pollutant molecules in the solution phase and on the outer adsorbent surfaces requires sufficient time. Besides, the internal diffusion time of pollutants through adsorbent pores and the adsorption process onto active sites inside pores should be considered [95]. Adsorption generally occurs rapidly at the beginning on the interface between the AC and the pollutant. Then, it slows down at the internal diffusion. The adsorption type, such as monolayer or multilayer formation, affects this phenomenon.

A higher concentration of dye substances is the driving force for the movement acceleration of dye molecules from the solution phase to the adsorbent surface [99]. Thus, interactions between the dye molecules or heavy metals and carbon surface improve, more water pollutants will be adsorbed, and adsorption equilibrium is attained more quickly. The adsorbent dose should also be increased to obtain more active sites for adsorption. However, under certain conditions, the increase in adsorbent dosage can reduce adsorption efficiency because of the potential reduction of active sites from the adsorbent molecule aggregations [100].

Activated carbons from *Camellia oleifera* seed shells and coffee husks have nice recyclability because they still have good adsorption capacity toward MB and Cr(VI) (>55%) after seven times use. It is higher than AC from bean dreg (Cr(VI)) and expired beverage (MB) which have adsorption capacities of <50% after five and four times regenerations, respectively. Then, activated carbon from peanut shells has different regeneration abilities by different activation agents. Activation using $ZnCl_2$ exhibits better performance after four cycles compared to activation with NaOH and steam. Furthermore, incorporating *Dodonaea viscosa* into calcium-alginate beads can improve the desorption percentage of MB adsorption.

3. Adsorption isotherms

An adsorption isotherm represents how a substance is adsorbed on an adsorbent as a function of equilibrium concentration and amount of adsorbed material at constant temperature. Besides that, this study describes how the mobility and retention of the pollutants enter porous adsorbents [101]. Hence, the adsorption mechanism can be described through assumptions on the adsorption isotherm models. General two-parameters isotherms models comprise Langmuir, Freundlich, Temkin, and Dubinin–Radushkevich. Besides that, there are three-parameters isotherm models, such as Redlich-Peterson, Langmuir-Freundlich, Toth, and Sips isotherm models. Table 4 displays the adsorption isotherm model and regression correlation coefficient of the activated carbons as water pollutant adsorbents. Adsorption isotherm types are distinguished based on the nature of the adsorbent surface, the propensity of the adsorbed phase on the adsorbent, the mathematical equation, and the shape of the adsorption curve.

There are three adsorption stages of dyes on the activated carbon. These consist of (1) diffusion of adsorbate molecules to adsorbent surface in the solution phase, (2) diffusion of adsorbate molecules into adsorbent pores, and (3) adsorption of those molecules on the active sites in internal pores [102]. Similar stages may occur for heavy metal adsorption. Three adsorption isotherm models that are often fitted to the experimental data in the studies of activated carbon-base water pollutant adsorbents are the Langmuir, Freundlich, Temkin, and Dubinin–Radushkevich models. Linear forms of adsorption isotherm equations are convenient and viable tools to identify and describe adsorption systems. The linear forms of these models are given in Equations 2, 3, 4 and 5, respectively [49, 53, 103].

$$\frac{C_\mathrm{e}}{q_\mathrm{e}} = \frac{1}{K_\mathrm{L} q_\mathrm{m}} + \frac{C_\mathrm{e}}{q_\mathrm{m}}, \tag{2}$$

$$\ln q_\mathrm{e} = \ln K_\mathrm{F} + \frac{1}{n}\ln C_\mathrm{e}, \tag{3}$$

$$q_e = \frac{RT}{b_\mathrm{T}}\ln C_e + \left(\frac{RT}{b_\mathrm{T}}\right)\ln K_\mathrm{T}, \tag{4}$$

$$\ln q_\mathrm{e} = \ln q_\mathrm{m} - K'\left(RT\ln\left(1+\frac{1}{C_\mathrm{e}}\right)\right)^2, \tag{5}$$

where C_e is the adsorbate concentration at equilibrium, q_m is the maximum adsorption capacity (mg·g^{-1}), q_e is the amount of adsorbed pollutants at equilibrium, $1/n$ is an empirical constant that measures adsorption intensity [59]. K_L (L·mg^{-1}) and K_F (L·mg^{-1}) are the Langmuir and Freundlich equilibrium constants in adsorption, K_T (L·mg^{-1}) and K' are the Temkin and Dubinin–Radushkevich equilibrium constants corresponding to binding energy and mean free energy of adsorption per molecule of adsorbate, respectively. The adsorption capacity and attractivity of the adsorbent can be determined by the K value [62]. b_T is the adsorption potential of the adsorbent, R is the universal gas constant (8.314 J.mol^{-1}·K^{-1}), and T is the absolute temperature (K).

The term $1/n$ in the Freundlich model is heterogeneity factor which corresponds to the deviation of the linear degree, adsorption intensity, and the objectives of adsorption [53, 65]. Adsorption takes place easily if $1/n < 1$ (specifically at a range of 0.1–0.5), whereas $1/n > 1$ indicates the difficulty of the adsorption process [53, 104]. Another source states that the value of n relates to the nature of adsorption process. Physisorption is highly possible if $n > 1$, whereas chemisorption must comply $n < 1$ [50]. Not only that, dimensionless separation factor (R_L) in Langmuir model corresponds to adsorption tendency, which consists of three categories, favorable ($0< R_L< 1$), unfavorable ($R_L > 1$), irreversible ($R_L = 0$), or linear ($R_L = 1$), respectively [105, 106]. The formula is expressed by Equation 6 [107]. All activated carbons in this review study show favorable adsorption toward water pollutants based on the R_L value.

$$R_L = \frac{1}{1+KC}. \tag{6}$$

However, linear isotherm models sometimes are not applied due to several error distributions. Thus, non-linear isotherm models are used to obtain better representations of experimental results [108,109]. The nonlinear equations of Langmuir, Freundlich, Temkin, Redlich-Peterson, Toth, Sips, Langmuir-Freundlich isotherms are represented by equations 7, 8, 9, 10, 11, 12 and, 13, respectively [110–114]:

$$q_e = \frac{q_{\mathrm{m}} K_a C_e}{1 + K_a C_e}, \tag{7}$$

$$q_{\mathrm{e}} = K_{\mathrm{F}}\, C_e^{\frac{1}{n}}, \tag{8}$$

$$q_{\mathrm{e}} = \frac{RT}{b_T} \ln\left(K_{\mathrm{T}} C_{\mathrm{e}}\right), \tag{9}$$

$$q_{\mathrm{e}} = \frac{K_{\mathrm{RP}}.\ C_e}{1 + a_{\mathrm{RP}}.\, C_e^{\beta_{\mathrm{RP}}}}, \tag{10}$$

$$q_{\mathrm{e}} = \frac{q_{\mathrm{m}}.\, K_{\mathrm{To}}.\ C_{\mathrm{e}}}{\left[1 + (K_{\mathrm{T}}.\, C_{\mathrm{e}})^{nT}\right]^{\frac{1}{nT}}}, \tag{11}$$

$$q_{\mathrm{e}} = \frac{q_{\mathrm{m}}.\ (K_{\mathrm{S}}.\, C_e)^{\frac{1}{nS}}}{1 + (K_{\mathrm{S}}.\, C_{\mathrm{e}})^{\frac{1}{nS}}}, \tag{12}$$

$$q_{\mathrm{e}} = \frac{qm_{\mathrm{LF}}.\ (K_{LF}.\, C_e)^{m\,LF}}{1 + (K_{\mathrm{LF}}.\, C_e)^{m\,LF}}, \tag{13}$$

where K_{RP}, K_{To}, and K_S are the Redlich-Peterson, Toth and Sips isotherm constants (L·mg^{-1}), A_{RP} and β_{RP} are the constant and the exponent in the Redlich-Peterson model, n_{T} and n_{S} are the heterogeneity factors and Sips isotherm exponent, respectively, qm_{LF}, K_{LF}, and m_{LF} are the Langmuir-Freundlich adsorption capacity, equilibrium constant related to heterogeneous sorbent, and heterogeneity parameter, respectively. Redlich-Peterson and Sips models also integrate the Freundlich and Langmuir isotherms. Redlich-Peterson model is capable of representing adsorption equilibrium conditions across a wide range of adsorbate concentrations and can be applied to both homogeneous and heterogeneous systems owing to its flexibility [115]. This model was developed to predict heterogeneous adsorption systems and overcome the limitations caused by increasing adsorbate concentration, which are encountered in the Freundlich isotherm model. Consequently, at low adsorbate concentrations, it behaves similarly to the Freundlich isotherm, while at high concentrations, it predicts monolayer adsorption, resembling the Langmuir isotherm [116]. The Toth isotherm model is a modification of the Langmuir model, designed to enhance the accuracy of predicted values in comparison to experimental results by considering the presence of submonolayer coverage. This model is used to describe adsorption on heterogeneous surfaces across a broad range of adsorbate concentrations, from low to high [117].

The determination or regression correlation coefficient (R^2) is used to identify the best isotherm model (Equation 14). Two isotherm models may simultaneously apply to the adsorption of pollutants by an activated carbon if their R^2 values are high (>0.9). The correlation coefficient was sometimes validated by the residual root mean squared error (RMSE) value expressed in Equation 15. The value of R^2 should be higher (near 1) to determine the isotherm model, whereas the RMSE value must be lower.

$$R^2 = 1 - \frac{\sum_{n=1}^{n} (q_{\mathrm{t.meas}} - q_{\mathrm{t.calc}})^2}{\sum_{n=1}^{n} (q_{\mathrm{t.calc}} - \overline{q_{\mathrm{t.calc}}})^2}, \tag{14}$$

$$RMSE = \sqrt{\frac{1}{n-1} \sum_{i=1}^{n} [q_{\mathrm{t.meas}} - q_{\mathrm{t.calc}}]^2}\,, \tag{15}$$

where $q_{t.meas}$ (mg·g^{-1}) and $q_{t.calc}$ (mg·g^{-1}) are experimental and calculated adsorption capacity of pollutants at specified time t, respectively. The n is the observation number. The suitability of the experimental and prediction adsorption capacities in each model is calculated by the average relative error (ARE%) using the following equation:

$$ARE = \frac{100}{n} \sum_{i=1}^{n} \left| \frac{|q_{\mathrm{e\ meas}} - q_{\mathrm{e\ calc}}|}{q_{e\ \mathrm{meas}}} \right| \ . \tag{16}$$

The suitability of the pollutant adsorption system with Langmuir isotherm, like activated carbon from dragon fruit peels, karanj fruit hulls, bagasse, cluster stalks, date pits, rice straw, banana peel, Australian pine cones, apple peel, peanut shell, cypress fruit, empty palm oil fruit bunches and carbide waste, oak cupules, spent brewery barley husks, and bean dreg indicates the monomolecular layer formation of pollutants on the homogenous surface. There was no interaction within adsorbates on the adsorbent sites, and they have equivalent energy. In contrast, adsorptions that follow the Freundlich model, like a bamboo chip, coconut shell, nutmeg shell, coffee ground, ziziphus lotus, and jengkol shell, are assumed to establish a multilayer on the heterogeneous surface of the adsorbent. Physical adsorption dominates this isotherm model, in which not all parts of adsorbent surfaces are occupied by pollutants [118]. Adsorption on the heterogenous solid is also explained by the Temkin isotherm model. This model assumes that the adsorption process is characterized by a uniform and decreasing adsorption heat that changes linearly with the increase in coverage of the adsorbent surface [114]. Adsoption of RR195 by activated carbon from Rice husk is an example that obeys this model. Dubinin–Radushkevich isotherm model (D-R model) corroborates the physisorption process of the methyl orange adsorption onto activated carbon from prickly pear seed cake through adsorption distribution on the heterogeneous surface [65]. In terms of physisorption, the adsorption of pollutants on the AC is reversible owing to weak interactions in the form of van der Waals forces. The D-R model can also determine the adsorption energy of the pollutant and AC to assess the most dominant type of ad-

DOI: 10.15826/chimtech.2025.12.2.14

sorption (physisorption or chemisorption). It is same with the free energy of adsorption.

Table 4 Source/type of activated carbon, Adsorption isotherm model, regression correlation coefficient from the optimum condition, and calculated adsorption capacities.

No.	Source /type of activated carbon	Adsorption isotherm model	R^2	q_e (mg·g^{-1})	Ref.
1	Phoenix dactylifera fruit (MB)	Linear and Non-linear Langmuir	0.997 0.999	Linear: 149.25 Non-linear: 146.29 at 50 °C	[48]
2	Karanj (*Pongamia pinnata*) fruit hulls (MB)	Non-linear Langmuir RMSE: 1.281	0.998	239.4 at 50 °C	[58]
3	Winemaking waste: Bagasse (MB)	Linear Langmuir $0 < RL < 1$	0.955	1156.65 at 80 °C	[59]
4	Winemaking waste: Cluster stalks (MB)	Linear Langmuir $0 < RL < 1$	0.972	1169.25 at 80 °C	[59]
5	Sunflower piths (MB)	NaOH: Non-linear Langmuir KOH: Non-linear Freundlich $n = 11.22$	0.899 0.912	965.40 369.19	[50]
6	Rice straw (MB)	KOH: Linear Langmuir H_3PO_4 Linear Freundlich $n = 2.45$ CO_2: Linear Freundlich $n = 0.47$ N_2: Linear Dubinin–Radushkevich	0.995 0.998 0.999 0.999	507.61 118.34 204.49 129.99	[49]
7	Rice straw (CR)	KOH: Linear Freundlich $n = 2.92$ H_3PO_4: Linear Freundlich $n = 1.72$ CO_2: Linear Freundlich n = 1.45 N_2: Linear Freundlich $n = 1.42$	0.989 0.997 0.997 0.959	258.40 617.28 740.74 641.02	[49]
8	Liquefied wood (MB)	Linear Langmuir	0.982	729.93	[53]
9	Coconut Shell (MB)	Hot air Linear Freundlich $n > 1$ H_3PO_4 Linear Freundlich $n > 1$	0.992 0.992	15.553 15.478	[61]
10	Rice straw (MB)	Linear Langmuir	0.999	9665 at 30 °C, pH 8	[62]
11	Dragon fruit peels (MB)	Non-linear Langmuir	0.999	195.2 at 50 °C	[63]
12	Bamboo chip (MB)	Non-linear Freundlich $n = 1.42$	0.96	305.3 at 40 °C	[64]
13	Prickly pear seed cake (MB and MO)	MB: Non-linear Freundlich $n = 12.31$ MO: Non-linear Freundlich $1/n = 0.29$	0.999 0.999	MB: 257.86 MO: 319.06	[65, 66]
14	Sugar scum powder (MO)	Linear Langmuir	0.99	15.24 (adsorbent dose:16 g/L; pH 7.21; 22 °C)	[67]
15	Rice husk (RR195)	Linear Temkin	0.99 at 25 °C	2.0	[68]
16	Eucalyptus wood chips (MB)	–	–	–	[69]
17	Spent coffee grounds (AY)	Linear Freundlich $1/n = 0.3483$	0.987	4.22	[70]
18	Seed hair fibers of metaplexis japonica (MB)	Linear Langmuir	0.997	943.37	[71]
19	Camellia oleifera seed shell (MB)	Non-linear Langmuir	0.965	541.42 at 55 °C	[72]
20	Cashew nut shell (BG)	Linear Langmuir $0 < RL < 1$	0.995	243.9	[74]

No.	Source /type of activated carbon	Adsorption isotherm model	R^2	q_e (mg·g^{-1})	Ref.
21	Coffee husk from Coffee arabica (MB)	Langmuir-Freundlich $1/n = 0.285$ RMSE: 0.42	0.9937	88.1	[75]
22	Dodonaea Viscosa (DV) into beads of calcium-alginate (ACAB) (MB)	DV: Linear Freundlich $1/n = 0.599$ ACAB: Linear Freundlich $1/n = 0.559$	0.998 0.995	29.41 333	[76]
23	Oak Cupules (NBB, CV)	NBB: Non-linear Langmuir CV: Non-linear Langmuir	0.992 0.935	213 625	[77]
24	Jengkol shell (Cu(II))	Linear Freundlich $1/n = 0.523$	0.946	104.167	[57]
25	Banana peel (Cu(II), Ni(II), and Pb(II))	Cu(II) Ni(II) Pb(II) Linear Langmuir 0 < RL< 1	0.934 0.953 0.833	13.81 20.88 –	[78]
26	Australian pine cones (Cu(II))	Linear Langmuir	0.954	12.82	[79]
27	Apple peel (Cr(VI))	Linear Freundlich $1/n = 0.6341$	0.99	36.01	[80]
28	Bean dreg (Cr(VI))	Linear Langmuir 0 < RL< 1	0.99	3.3 mmol·g^{-1}	[81]
29	Elm tree (Cr(VI) and Pb(II))	Linear Langmuir 0 < RL< 1 Pb(II) ARE: 40.7% Cr(VI) ARE: 12.3%	0.98	Pb(II): 232.56 Cr(VI): 113.63	[82]
30	Pistachio wood (Pb(II))	Non-linear Langmuir (RMSE: 1.186) (ARE: 0.022%) Non-linear Redlich-Peterson (RMSE: 1.16) (ARE: 0.024%) Non-linear Sips (RMSE: 1.130) (ARE: 0.027%) Non-linear Toth (RMSE: 1.112) (ARE: 0.026%)	0.999 0.999 0.999 0.999	190.2 367.5 188.9 188.3	[52]
31	Carrot, tomato, and polyethylene terephthalate composite (Co(II))	Linear Langmuir	0.97	312.5	[83]
32	Camellia oleifera seed shell (Cr(VI))	Non-linear Freundlich $1/n = 0.09$	0.96	250.97 at 45 °C	[72]
33	Avocado seed biomass (Cr(VI) and Pb(II))	Cr(VI): Non-linear Langmuir Pb(VI): Non-linear Freundlich $n = 1.7$	0.912 0.921	5.10 26.6	[84]
34	Empty palm oil fruit bunches and carbide waste (Fe(II))	Linear Langmuir 0 < RL< 1	0.995	2.256	[85]
35	Ziziphus lotus (Cd and Cr(VI))	Cd: Freundlich $1/n = 0.868$ Cr(VI): Freundlich $1/n = 0.652$	0.937 0.997	23.256 17.857	[86]
36	Coffee grounds (Cd and Cr(VI))	Cd: Freundlich $1/n = 0.482$ Cr(VI): Freundlich $1/n = 0.612$	0.995 0.967	8.849 10.526	[86]
37	Nutmeg shell (Pb(II) and Cu(II))	Pb(II): Linear Freundlich $n = 0.99$ Cu(II): Linear Freundlich $n = 0.6746$	0.976 0.988	9.603 0.035	[87]
38	Coconut shell (Fe(II) and Pb(II))	Fe(II): Linear Freundlich $1/n = 0.774$ Pb(II): Linear Freundlich $1/n = 0.814$	0.998 0.996	–	[88]
39	Peanut shell (Pb(II) and MB)	MB:	0.999	500.00	[73]

No.	Source /type of activated carbon	Adsorption isotherm model	R^2	q_e (mg·g^{-1})	Ref.
		NaOH: Linear Langmuir	0.999	248.33	
		ZnCl$_2$: Linear Langmuir	1.00	333.33	
		Steam: Linear Langmuir			
		Pb(II): Steam: Linear Langmuir 0 < RL< 1	0.999	130.89	
40	Cypress fruit (Pb(II), Co(II), and Cd(II))	Pb(II): Linear Langmuir Co(II): Linear Langmuir Cd(II): Linear Langmuir	0.997 0.993 0.995	84.15 79.16 61.32	[89]
41	Spent brewery barley husks (Cd(II))	Non-Linear Langmuir	0.775	6.64	[90]
42	Expired beverages (MB)	Linear Langmuir	0.997	413.43 at 55 °C	[95]
43	Waste carpets (MB)	Linear Langmuir 0 < RL< 1	0.993	769.2	[91]
44	Activated carbon with Zinc from electric arc furnace dust (RB19 and CY3247)	Linear Langmuir for RB19 and CY3247	0.998 at 60 °C	RB19: 84.03 CY3247: 72.46	[92]
45	Denim fabric residue (Pb(II))	Non-Linear Langmuir for cellulose and cellulose-polyester	0.97	Cellulose: 361.54 cellulose-polyester: 385.77	[54]
46	Fe_3O_4-waste paper activated carbon composite (MB)	Linear Langmuir	0.967	101	[93]
47	Activated charcoal (AB and BB)	Linear Langmuir	AB: 0.98 BB: 0.99	–	[94]
48	Waste paper (MB and Cr(VI))	H_2O MB: Non-Linear Freundlich (RMSE:6.115) Cr(VI): Non-Linear Freundlich (RMSE: 7.829) HNO_3 MB: Non-Linear Freundlich (RMSE: 5.812) Cr(VI): Non-Linear Freundlich (RMSE: 7.937) $KMnO_4$ MB: Non-Linear Freundlich (RMSE: 8.103) Cr(VI): Non linear Freundlich (RMSE: 9.520)	H_2O_2 MB: 0.993 Cr(VI): 0.991 HNO_3 MB: 0.995 Cr(VI): 0.997 $KMnO_4$ MB: 0.996 Cr(VI): 0.995	H_2O_2 MB: 1.21 Cr(VI): 1.06 HNO_3 MB: 1.227 Cr(VI): 1.105 $KMnO_4$ MB: 1.199 Cr(VI): 1.164	[96]
49	Date palm spikelets (MO) (MO =200 mg·L–1)	Non-linear Langmuir at 40 °C Non-linear Freundlich at 20 °C (1/*n* = 0.201, NSD: 0.02)	0.983 0.981	215.29 (NSD: 5.42)	[97]

Notes:

MB	: Methylene blue	AB	: Acid blue;
CR	: Congo Red	BB	: Basic blue;
–	: Not mentioned.		

Activated carbon produced from rice straw exhibits a good fit with both the Langmuir and Dubinin–Radushkevich isotherm models. It indicates similar adsorption behavior, although the surface of AC is heterogeneous [119]. Although not following the Langmuir model, the adsorption capacity of AC was still calculated by the Langmuir equation.

The activated carbons that obey Langmuir adsorption isotherm can adsorb pollutants through electrostatic interaction, π-π interaction, and hydrogen bonding [63]. This adsorption process is based on functional groups or heteroatoms in the activated carbon. An example is the hydroxyl group (–OH). This group has a positive charge at lower pH (pH < 7), but it changes slowly to a negative charge by increasing pH. The electrostatic attraction occurs when a pollutant has different charges to the activated carbon surface in acid or base conditions. In addition, activated carbon, which contains hydroxyl groups, also tends to form hydrogen bonding and/or π-π interactions with dye molecules since they are similar to organic compounds. On the contrary, repulsion forces refer to the interaction between adsorbent and pollutants with similar charges, decreasing the dye and heavy metal adsorptions on the AC surface.

4. Adsorption thermodynamics

This part explains the effect of temperature, adsorption energy, and reaction spontaneity on dyes and heavy metals adsorption. Higher temperatures can increase the collision frequency as well as adsorption process from the diffusion stages to physical and/or chemical bonding formation. In this condition, pollutant adsorption is an endothermic reaction ($\Delta H^o_{ads} > 0$). On the other hand, a negative value of ΔH^o_{ads} indicates releasing energy in the adsorption process of pollutants by activated carbon (exothermic process) [120]. Thermodynamic parameters, for instance, Gibbs free energy change of adsorption (ΔG^o_{ads}), the standard enthalpy change of adsorption (ΔH^o_{ads}), adsorption entropy change (ΔS^o_{ads}), and the equilibrium constant of adsorption (K_a) are discussed in this section. These parameters are described by Equations 17, 18, 19, and 20. They are usually determined in adsorption studies for various sources of activated carbons. Table 4 displays the source of activated carbon and the values of thermodynamic parameters. The value of ΔS^o_{ads} relates to the orderliness of pollutant adsorption on the surface. $\Delta S^o_{ads} > 0$ indicates a more random surface system. In this condition, structural changes on the interface of activated carbon and dyes/heavy metals occur during the adsorption process due to the release of water molecules from the adsorbent surface [48, 121]. Otherwise, a negative value of entropy change ($\Delta S^o_{ads} < 0$) indicates a less random system [122]. Meanwhile, the spontaneity and the adsorption type (physisorption or chemisorption) are investigated by ΔG^o_{ads} parameter. The negative value of ΔG^o_{ads} obtained after raising the temperature means that adsorption is favorable and vice versa. Good pollutant adsorption at higher temperatures refers to the chemisorption forming strong chemical bonds. In contrast, physisorption is related to the van der Waals interaction, for instance, dipole-dipole, dipole-ion, electrostatic interaction, and London dispersion forces.

$$\Delta G^o = -RT \ln K_a, \tag{17}$$

$$\Delta H^o = R\frac{T_1.T_1}{T_2 - T_1} 2.303 \log \frac{b_2}{b_1} (\text{for Langmuir}), \tag{18}$$

$$\Delta S^o = \frac{\Delta H^o - \Delta G^o}{T}, \tag{19}$$

$$K_a = \frac{C_s}{C_e}. \tag{20}$$

C_s is the adsorbate concentration (dye or heavy metal) calculated from the difference between the initial concentration and equilibrium concentration (C_e) of the adsorbate. T is temperature, R is the universal gas constant (8.314 J·mol⁻¹·K⁻¹), b_1 and b_2 are Langmuir constants at T_1 and T_2. The adsorption equilibrium constant (K_a) is similar to the Langmuir equilibrium constant if the adsorption isotherm obeys the Langmuir model [123]. In addition, ΔH^o and ΔS^o can also be calculated from the gradient and intercept of the Van't Hoff equation:

$$\ln K_a = \frac{-\Delta H^o}{RT} + \frac{\Delta S^o}{R}. \tag{21}$$

Activated carbons from rice straw, bagasse, and cluster stalks showed a positive shift of ΔG^o_{ads} at high temperature toward methylene blue adsorption. Hence, thermodynamically, the adsorption capacities of these activated carbons decrease at higher temperatures. Conversely, MB adsorptions by AC from phoenix dactylifera fruit, prickly pear seed cake, coffee husk, and peanut shells show a negative shift of ΔG^o_{ads} in higher temperatures. Pb(II) adsorption by activated carbon from pistachio wood also gets stronger with increasing temperature. Adsorption of methyl orange with sugar scum has a relatively temperature-independent ΔG^o_{ads}. Thus, temperature changes do not have a significant impact. The threshold values of ΔG^o_{ads} are listed below [124]:

$\Delta G^o_{ads} =$ negative (adsorption is spontaneous and thermodynamically favorable).

$\Delta G^o_{ads} =$ positive (adsorption is not spontaneous).

$\Delta G^o_{ads} =$ −20 kJ·mol⁻¹ and more positive (physisorption).

$\Delta G^o_{ads} =$ −20 to −80 kJ·mol⁻¹ (physisorption and chemisorption).

$\Delta G^o_{ads} =$ −80 kJ·mol⁻¹ and more negative (chemisorption).

Table 5 Optimum conditions of Equilibrium constant (K_{ads}), the standard enthalpy change (ΔH^o_{ads}), adsorption entropy change (ΔS^o_{ads}), and Gibbs free energy change of adsorption (ΔG^o_{ads}) from the adsorption of water pollutants by various sources of activated carbons.

No.	Source /type of activated carbon	K_{ads}	ΔH^o_{ads} (kJ·mol⁻¹)	ΔS^o_{ads} (kJ·mol⁻¹K⁻¹)	ΔG^o_{ads} (kJ·mol⁻¹)	Ref.
1	Phoenix dactylifera fruit (MB)	0.101 L·mg⁻¹	6.182	21.19	−7.797 at 50°C	[48]
2	Karanj (Pongamia pinnata) fruit hulls MB)	0.071 L·mg⁻¹	38.885	0.130	−2.841 at 50°C	[58]
3	Winemaking waste: Bagasse (MB)	–	−49.25	−0.51 at 30 °C	−11.94 at 30 °C	[59]
4	Winemaking waste: Cluster stalks (MB)	–	−37.89	−0.005 at 30 °C	−14.40 at 30 °C	[59]
5	Sunflower piths (MB)	NaOH: 1.612 L·mg⁻¹	–	–	–	[50]
6	Rice straw (MB)	KOH: 3.97 L·mg⁻¹	–	–	–	[49]
7	Rice straw (CR)	–	–	–	–	[49]
8	Liquefied wood by	0.96 L·mg⁻¹	–	–	–	[53]

No.	Source /type of activated carbon	K_{ads}	ΔH^{o}_{ads} (kJ·mol^{-1})	ΔS^{o}_{ads} (kJ·mol^{-1}K^{-1})	ΔG^{o}_{ads} (kJ·mol^{-1})	Ref.
	$ZnCl_2$ activation					
9	Coconut Shell (*Cocous Nucifera L.*) (MB)	–	–	–	–	[61]
10	Rice straw (MB)	54.753 at 20 °C, pH 6	–	–	−9.751 at 20 °C, pH 6	[62]
11	Dragon fruit peels (MB)	1.32 L·mg^{-1} at 50 °C	–	–	–	[63]
12	Bamboo chip (MB)	–	–	–	–	[64]
13	Prickly pear seed cake (MB and MO)	MB: – MO: –	MB: 9.66 MO: –	MB:0.0826 MO: –	MB: −33.96 at 20 °C MO: –	[65,66]
14	Sugar scum powder (MO)	2.622 L·mg^{-1}	−14.14	0.00203	−14.63 at 20 °C	[67]
15	Rice husk (RR195)	–	Positive (+) value	Negative (−) value	Positive (+) value at 25 °C	[68]
16	Eucalyptus wood chips (MB)	–	–	–	–	[69]
17	Spent coffee grounds (AY)	–	–	–	–	[70]
18	Seed hair fibers of metaplexis japonica (MB)	0.012 at 25 °C	–	–	–	[71]
19	Camellia oleifera seed shell (MB)	MB: 11.45 at 45 °C	–	–	–	[72]
20	Cashew nut shell (BG)	0.1782 L.g^{-1}	–	–	–	[74]
21	Coffee husk from Coffee arabica (MB)	–	−8.77 at 30 °C	121.35 at 30 °C	−31.67 at 60 °C	[75]
22	Dodonaea Viscosa (DV) into beads of calcium-alginate (ACAB) (MB)	–	DV: 10.9 at 20 °C ACAB: 19.1 at 20 °C	0.00594 at 20 °C 89.087 at 20 °C	−5.642 at 60 °C −12.091 at 70 °C	[76]
23	Oak Cupules (NBB and CV)	NBB: 0.2814 CV: 0.2462	37.15 60.75	0.138 0.224	−16.06 at 40 °C −113.8 at 40 °C	[77]
24	Jengkol shell (Cu(II))	0.391 L.g^{-1}	−1.914	−0.141	45.172 at 45 °C	[57]
21	Banana peel (Cu(II), Ni(II), and Pb(II))	Cu(II): 0.69 L·mg^{-1} Ni(II): 0.324 L·mg^{-1} Pb(II): –	–	–	–	[78]
22	Australian pine cones (Cu(II))	42.93 L·g^{-1}	–	–	–	[79]
23	Apple peel (Cr(VI))	–	8.326	0.0331	−2.05 at 40 °C	[80]
24	Bean dreg (Cr(VI))	2.40 L·mmol^{-1}	–	–	–	[81]
25	Elm tree (Cr(VI) and Pb(II))	Pb(II): 0.42 L·mg^{-1} Cr(VI): 0.184 L·mg^{-1}	–	–	–	[82]
26	Pistachio wood (Pb(II))	1.983 L·g^{-1}	30.761	0.211	−38.338 at 55 °C	[52]
27	Carrot, tomato, and polyethylene terephthalate (Co(II))	0.0016 L·g^{-1}	–	–	–	[83]
28	Camellia oleifera seed shell (Cr(VI))	–	–	–	–	[72]
29	Avocado seed biomass (Cr(VI) and Pb(II))	Cr(VI): 490 L·g^{-1} PB(II): –	–	–	–	[84]
30	Empty palm oil fruit bunches and carbide waste (Fe(II))	0.263 at 27 °C	–	–	–	[85]
31	Ziziphus lotus (Cd and Cr(VI))	–	Cd: 6.102 Cr(VI): 8.937	Cd: 24.136 Cr(VI): 25.681	Cd: −7.788 Cr(VI): −8.286	[86]
32	Coffee grounds (Cd and Cr(VI))	–	Cd: 11.191 Cr(VI): 8.597	Cd: 14.358 Cr(VI): 15.447	Cd: −5.626 Cr(VI): −4.981	[86]
33	Nutmeg shell (Pb(II) and Cu(II))	–	–	–	–	[87]
34	Coconut shell (Fe(II) and Pb(II))	–	–	–	–	[88]
35	Peanut shell (Pb(II) and MB)	MB NaOH: 0.119 $ZnCl_2$: 0.061 Steam: 0.098	MB NaOH: 7.89 $ZnCl_2$: 13.71 Steam: 12.89	MB NaOH: 0.145 $ZnCl_2$: 0.157 Steam: 0.159	MB NaOH: −39.10 $ZnCl_2$: −37.31 Steam: −38.58	[73]

DOI: 10.15826/chimtech.2025.12.2.14

No.	Source /type of activated carbon	K_{ads}	ΔH^o_{ads} (kJ·mol^{-1})	ΔS^o_{ads} (kJ·mol^{-1}K^{-1})	ΔG^o_{ads} (kJ·mol^{-1})	Ref.
		Pb(II) Steam: 0.037	Pb(II): –	Pb(II): –	at 50 °C Pb(II): –	
36	Cypress fruit (Pb(II), Co(II), and Cd(II))	Pb(II): 1.072 Co(II): 0.136 Cd(II): 0.162	Pb(II): 22.24 Co(II): 21.28 Cd(II): 34.26	Pb(II): 33.22 Co(II): 17.76 Cd(II): 56.12	Pb(II): 11.79 Co(II): 15.46 Cd(II): 16.57 At at 45 °C	[89]
37	Spent brewery barley husks (Cd(II))	1.08 L$^{1/n}$ g^{-1} mg$^{1/n}$	–87.612	–0.294	–87.61 at 25°C	[90]
38	Waste carpets (MB)	17.5 at 25 °C	–29.744 at 25°C	–0.076 at 25°C	–7.09 at 25°C	[91]
39	Activated carbon with Zinc from electric arc furnace dust (RB19 and CY3247)	RB19: 0.54 L·mg^{-1} CY3247: 0.53 L·mg^{-1} At 60 °C	–	–	–	[92]
40	Denim fabric residue (Pb(II))	Cellulose: 0.36 Cellulose-polyester: 0.14	Cellulose: –75.93 Cellulose polyester: –82.03	Cellulose: –0.194 Cellulose-polyester: –0.232	Cellulose: –19.43 Cellulose-polyester: –19.18	[54]
41	Fe_3O_4-waste paper activated carbon composite	–	24.66	0.0872	–2.956 at 45 °C	[93]
42	Activated charcoal	–	46.66	–0.06	–43.56 at 30 °C	[94]
43	Expired beverage (MB)	21.598 L·g^{-1}	19.584	0.0922	–1.755	[95]
44	Waste paper (MB and Cr(VI))	–	H_2O_2 MB: 36.63 Cr(VI): 41.15 HNO_3 MB: 29.44 Cr(VI): 34.07 $KMnO_4$ MB: 30.38 Cr(VI): 36.63	H_2O_2 MB: 0.477 Cr(VI): 0.540 HNO_3 MB: 0.423 Cr(VI): 0.506 $KMnO_4$ MB: 0.432 Cr(VI): 0.511	H_2O_2 MB: –53.75 Cr(VI): –55.37 HNO_3 MB: –42.98 Cr(VI): –46.80 $KMnO_4$ MB: –45.66 Cr(VI): –51.36 at 25 °C	[96]
45	Date palm spikelets (MO) (MO =200 mg·g^{-1})	0.43 at 20 °C	73.9 at 20 °C	0.3513 at 20 °C	–35.89 at 40 °C	[97]

–: not mentioned.

5. Adsorption kinetics

The achievement of the adsorption equilibrium of the AC depends on the diffusion rate of dye molecules and heavy metals from the solution to the AC surface until occupying porous structures. The adsorption rate is usually faster at the beginning due to the high surface area of the adsorbent which provides a large number of binding sites to interact with water pollutants [54]. Then, it decreases slowly. For instance, the adsorption equilibrium of AC from Australian pine cones, bean dreg, liquefied wood, and Karanj fruit hulls was reached after 2 h, 3 h, 5h, and 24 h, respectively. Meanwhile, thermal tension treatment can significantly accelerate Pb(II) and Cr(VI) uptake due to the development of adsorption sites on the AC surface [82].

The kinetic study investigates pollutant's adsorption rate and reaction order of adsorption for activated carbon-based adsorbents. This study depends on the contact time of the experiments. The adsorption capacity obtained from calculations in a kinetic study is compared to the adsorption capacity obtained from other calculations, such as batch adsorption tests and the adsorption isotherm equations. Generally, two kinetic equations used for explaining the adsorption pattern are pseudo-first-order and pseudo-second-order. Pseudo-first-order kinetics represent frontier diffusion from the adsorption process. It is shown by the adsorption of water pollutants by AC from dragon fruit peels, spent coffee ground, and ziziphus lotus. Meanwhile, the adsorption process, which is determined by the entire stages of adsorption, certainly obeys pseudo-second-order kinetics. The linear forms of those equations are as follows:

$$\ln(q_e - q_t) = \ln q_e - k_1 t, \tag{22}$$

$$\frac{t}{q_t} = \frac{1}{k_2 q_e^2} + \frac{t}{q_e}, \tag{23}$$

where k_1 and k_2 are the rate constant of a pseudo-first-order (h^{-1}) and pseudo-second-order (g·mg^{-1}·h^{-1}), respectively, q_e and q_t refer to the amounts of dye adsorbed at equilibrium and at a specified time (mg·g^{-1}) respectively, and t represents time (h). The non-linear forms of the kinetic models were also used, owing to being regarded as better for predicting kinetic parameters [66, 67]. These nonlinear equations of pseudo-first-order and pseudo-second-order are given in the following equations [65, 125]:

$$q_t = q_e(1 - e^{-k_1 t}), \tag{24}$$

$$q_t = \frac{k_2 q_e^2 t}{1 + k_2 q_e t}. \quad (25)$$

Other kinetic equations that correspond to the adsorption capacity are the Elovich and Avrami equations. They describe interaction on the heterogeneous surface that is predominantly affected by chemical adsorption and reaction that is centered on the active sites of the solid surface [126, 127], but it is not entirely a rate-determining step. Elovich and Avrami equations are expressed as follows [50]:

$$q_t = \frac{1}{\beta}\ln(1 + \alpha\beta t), \quad (26)$$

$$q_t = q_{\mathrm{av}}(1 - e^{(k_{\mathrm{av}}t)})^{n_{\mathrm{av}}}. \quad (27)$$

The term β is the desorption constant ($\mathrm{mg \cdot g^{-1}}$) correlated to widening coverage and activation energy of chemisorption, and α is the initial rate of adsorption ($\mathrm{mg \cdot g^{-1} min^{-1}}$). Then, q_{av} is the theoretical adsorption capacity of Avrami ($\mathrm{mg \cdot g^{-1}}$), q_t is the adsorption capacity at time t ($\mathrm{mg \cdot g^{-1}}$), k_{av} is the Avrami constant rate, and n_{av} is the Avrami order model.

The best-fitted model is determined by the coefficient of determination (R^2), equation 14. Sometimes, two nonlinear error functions, normalized standard deviation (NSD) and average relative error (ARE) are also used to determine the order of the adsorption kinetics. The equations are expressed as follows [58]:

$$\mathrm{NSD} = 100\ x \sqrt{\frac{1}{n-1}\sum_{i=1}^{n}\left[\frac{q_{\mathrm{t.meas}} - q_{\mathrm{t.calc}}}{q_{\mathrm{t.calc}}}\right]^2}, \quad (28)$$

$$\mathrm{ARE} = \frac{100}{n}\sum_{i=1}^{n}\left[\frac{q_{\mathrm{t.meas}} - q_{\mathrm{t.calc}}}{q_{\mathrm{t.calc}}}\right]. \quad (29)$$

The best-fitted order is based on the lowest values of NSD and ARE. Meanwhile, the activation energy of adsorption ($\mathrm{kJ \cdot mol^{-1}}$) is determined by the Arrhenius equation as follows:

$$\ln K = \ln A - \left(\frac{E_a}{RT}\right), \quad (30)$$

where K is the kinetic constant at a specified temperature (K), A is the Arrhenius constant, and R is the universal gas constant.

Adsorption kinetics is determined by fitting the equations above. Adsorption by activated carbons from waste carpet, winemaking wastes, liquefied wood, coconut shell, jengkol, cypress fruit, dodonaea viscosa, and apple peel follows a pseudo-second order. Adsorption kinetics in this condition indicates the chemisorption process as the rate-determining step in which adsorbent and adsorbate share and/or exchange electrons with each other [128]. The mechanism is initiated by external liquid film diffusion (stage 1), surface adsorption (stage 2), intra-particle diffusion in macropores and micropores until reaching equilibrium (stage 3) [91]. Hence, the number of active sites on the AC is directly proportional to the adsorption rate [129]. The decrease of the rate constant of pseudo-second-order by increasing adsorbent dosages indicates that the calculation of theoretical adsorption equilibrium by pseudo-second-order adsorption kinetics is almost similar to the experimental adsorption equilibrium [53]. A significant difference between theoretical and actual pollutant adsorption at equilibrium implies utilizing another kinetic order to describe the adsorption process. Besides external diffusion, the adsorption is also determined by intraparticle diffusion on the porous surface of adsorbents. Weber and Morris particularly expressed a model to observe intraparticle diffusion resistance. It is represented by internal micropore filling marked by a high determination coefficient (R^2) based on the linear plot in Equation 31. In adsorbents with various pore sizes, mass transfer is preceded by macropores and/or mesopores with a relatively high rate constant (k_{ed}), then followed by mass transfer through micropores with a lower rate constant (k_{id}), which $k_{\mathrm{ed}} > k_{\mathrm{id}}$ [130]:

$$q_t = k_{id}t^{1/2} + c, \quad (31)$$

where q_t ($\mathrm{mg \cdot g^{-1}}$) is adsorbed pollutant at time t (minute), k_{id} ($\mathrm{mg \cdot g^{-1} \cdot min^{-1/2}}$) is the adsorption rate constant of the intraparticle diffusion model, and c is a constant referred to the thickness of the boundary layer ($\mathrm{mg \cdot g^{-1}}$).

The linear plot of q_t vs $t^{1/2}$ implies the intraparticle diffusion as the sole rate-limiting step of the adsorption processes. Besides that, intercept and gradient obtained from the plots yield k_{id} and c. On the other hand, another mechanism may be rate-determining in the adsorption process when the intraparticle diffusion plot is not linear or multi linear, for instance, film diffusion [67]. It can be analyzed by the linear form of the Boyd model as follows:

$$\ln\left(1 - \frac{q_t}{q_e}\right) = -k_{\mathrm{fd}}t, \quad (32)$$

where k_{fd} is the liquid film diffusion constant obtained from the gradient of the linear plots between $\ln(1-q_t/q_e)$ and t. The comparison of R^2 values between the Weber-Morris and Boyd models is used to decide diffusion type, which is the rate-determining step of the pollutant adsorption onto AC [131].

6. Limitations

Numerous researchers in various countries have carried out studies on activated carbon-based adsorbents to overcome water pollutants. There are two methods that can be used to obtain good adsorbents: physical adsorption, which reduces the use of chemical substances, and chemical activation, which reduces energy consumption. Some even use both. Hence, further study requires more effective, efficient, and safe activation methods. Some studies did not include measurements of thermodynamic parameters.

Table 6 Kinetic parameters of the activated carbon from natural sources and waste as water pollutant adsorbents followed by calculated adsorption capacities.

No.	Source /type of activated carbon	Reaction order	R^2 (reaction order)	R^2 (Weber and Moris)	R^2 (Boyd Model)	ECT and E_a	q_e (mg·g–1)	Ref.
1	Phoenix dactylifera fruit (MB)	Pseudo-second order	0.99	0.8396	–	10 h	113.63	[48]
2	Karanj (*Pongamia pinnata*) fruit hulls (MB)	Pseudo-second order	0.99	0.985	0.994	24 h	150.85	[58]
3	Winemaking waste: Bagasse (MB)	Pseudo-second order	0.999	–	–	4 h −10.59 kJ·mol^{-1}	507.60 (30 °C)	[59]
4	Winemaking waste: cluster stalks (MB)	Pseudo-second order	0.999	–	–	3 h −12.09 kJ·mol^{-1}	505.05 (30 °C)	[59]
5	Sunflower piths (MB)	Pseudo-first order in low concentration of MB (500 mg·L^{-1}) Elovich model in high concentration of MB (1000 mg·L^{-1})	0.997 0.972	0.993 (1000 mg·L^{-1})	–	3 h	509.1	[50]
6	Rice straw (MB)	–	–	–	–	–	–	[49]
7	Rice straw (CR)	–	–	–	–	–	–	[49]
8	Liquefied wood (MB= 600 mg·L^{-1})	Pseudo-second order	0.999	–	–	5 h	725.63	[53]
9	Coconut shell (*Cocos Nucifera L.*) (MB)	Pseudo-second order	0.95 for phys. activ. 0.99 for chem.activ.	–	–	40 min for phys. activ. 60 min for chem. activ.	–	[61]
10	Rice straw (MB)	–	–	–	–	–	–	[62]
11	Dragon fruit peels (MB =200 mg·L^{-1})	Pseudo-first order	0.97	0.68	–	5 h	164.8	[63]
12	Bamboo chip (MB= 200 mg·L^{-1})	Pseudo-first order and Pseudo-second order	0.99	–	–	1 h	107.2	[64]
13	Prickly pear seed cake (MO and MB)	Pseudo-second order (for MO and MB)	0.998	Not linear for MO and MB	–	2 h for MO	200.34 for MO	[65, 66]
14	Sugar scum powder (MO= 100 mg·L^{-1})	Pseudo-second order	0.99	–	–	1 h	5.49	[67]
15	Rice husk (RR195)	Pseudo-second order	≈1	–	–	2 h	–	[68]
16	Eucalyptus wood chips (MB)	–	–	–	–	–	–	[69]
17	Spent coffee grounds (AY)	Pseudo-first order	0.983	–	–	–	–	[70]
18	Seed hair fibers of metaplexis japonica (MB)	–	–	–	–	–	–	[71]
19	Camellia oleifera seed shell (MB)	Pseudo-second order	0.99	–		3 h	476.19	[72]
20	Cashew nut shell (BG)	–	–	–	–	–	–	[74]
21	Coffee husk from Coffee arabica (MB)	Pseudo-first order	0.981	–	–	60 min	21.75	[75]
22	Dodonaea viscosa (DV) into beads of calcium-alginate (ACAB) (MB)	DV: Pseudo-second order ACAB: Pseudo-second order	0.997 0.99	0.975 0.97	–	70 min	9.1 7.8	[76]
23	Oak cupules (AD, NBB, CV)	NBB: Pseudo-first order CV: Pseudo-second order	0.992 1.0	0.947 0.713	–	180 min 90 min	125 333	[77]
24	Jengkol shell (Cu(II))	Pseudo-second order	0.998	–	–	75 min. −1.954	96.15	[57]

DOI: 10.15826/chimtech.2025.12.2.14

No.	Source /type of activated carbon	Reaction order	R^2 (reaction order)	R^2 (Weber and Moris)	R^2 (Boyd Model)	ECT and E_a	q_e (mg·g–1)	Ref.
25	Banana peel (Cu(II), Ni(II), and Pb(II))	–	–	–	–	–	–	[78]
26	Australian pine cones (Cu(II))	Pseudo-second order	0.985	–	–	2 h	27.03	[79]
27	Apple peel (Cr(VI))	Pseudo-second order	0.988	–	–	–	26.95	[80]
28	Bean dreg (Cr(VI))	Pseudo-second order	0.998	–	–	3 h	2.2 mmol·g^{-1}	[81]
29	Elm tree (Cr(VI) and Pb(II))	Pseudo-second order	Cr(VI): 0.99 Pb(II): 1.0	Cr(VI): 0.84 Pb(II): 0.81	–	Cr(VI): 60 min Pb(II): 30 min	Cr(VI): 108.7 Pb(II): 120.4	[82]
30	Pistachio wood (Pb(II))	Pseudo-second order	1.0 RMSE: 1.701 ARE: 0.017%	–	–	30 min	178.4	[52]
31	Carrot, tomato, and polyethylene terephthalate composite (Co(II))	Pseudo-second order	0.99	–	–	99 min	454.54	[83]
32	Camellia oleifera seed shell (Cr(VI))	Pseudo-second order	0.99			9 h	294.12	[72]
33	Avocado seed biomass (Cr(VI) and Pb(II))	Cr(VI): Pseudo-first order Pb(II): Pseudo-second order	Cr(VI: 0.986 Pb(II): 0.989	–	–	1.5 h	Cr(VI): 6.5 Pb(II): 26.3	[84]
34	Empty palm oil fruit bunches and carbide waste (Fe(II))	–	–	–	–	–	–	[85]
35	Ziziphus lotus (Cd and Cr(VI))	Cd: Pseudo-first order Cr(VI): Pseudo-first order	Cd: 0.99 Cr(VI): 0.99	–	–	2 h	Cd: 11.448 Cr(VI): 9.259	[86]
36	Coffee grounds (Cd and Cr(VI))	Cd: Pseudo-first order Cr(VI): Pseudo-first order	Cd: 0.99 Cr(VI): 0.99	–	–	2 h	Cd: 6.179 Cr(VI): 6.098	[86]
37	Nutmeg shell (Pb(II) and Cu(II))	–	–	–	–	–	–	[87]
38	Coconut shell (Fe(II) and Pb(II))	Fe(II): Pseudo-second order Pb(II): Pseudo-second order	Fe(II): 0.996 Pb(II): 0.997	–	–	4 h	Fe(II): 3.60 Pb(II): 4.27	[88]
39	Peanut shell (Pb(II) and MB)	MB: NaOH, ZnCl$_2$, and Steam: Pseudo-second order Pb(II): Steam: Pseudo-second order	0.999 0.999	MB NaOH: 0.749 ZnCl$_2$: 0.789 Steam: 0.660 Pb(II) Steam: 0.601	MB NaOH:0.978 ZnCl$_2$: 0.935 Steam:0.998 Pb(II) Steam: 0.864	MB NaOH: 1.5 h ZnCl$_2$: 45 min. Steam: 1.5 h Pb(II) Steam: 1.5 h	MB NaOH: 344 ZnCl$_2$: 52.0 Steam: 163.93 Pb(II) Steam:41.08	[73]
40	Cypress fruit (Pb(II), Co(II), and Cd(II))	Pseudo-second order	Pb(II): 0.996 Co(II): 0.999 Cd(II): 0.954	Pb(II): 0.843 Co(II): 0.462 Cd(II): 0.887	–	Pb(II): 1.5 h Co(II): 1.5 h Cd(II: 2 h	–	[89]
41	Spent brewery barley husks (Cd(II))	Pseudo-first order	0.951	–	–	5 min	5.0	[90]
42	Waste carpets (MB) (MB= 700 mg·L^{-1})	Pseudo-second order	0.997	–	–	12 h	718.3	[91]
43	Activated carbon with Zinc from electric arc furnace dust	Pseudo-second order	RB19: 0.999 CY3247:	RB19: 0.8425 CY3247:	–	45 min	RB19: 51.55 CY3247: 49.75	[92]

No.	Source /type of activated carbon	Reaction order	R^2 (reaction order)	R^2 (Weber and Moris)	R^2 (Boyd Model)	ECT and E_a	q_e (mg·g–1)	Ref.
	(RB19 and CY3247)		0.998	0.8432				
44	Denim fabric residue (Pb(II))	Pseudo-second order	0.999	Cellulose: 0.998 Cellulose-polyester: 0.992	–	5 min	Cellulose: 369.18 Cellulose-polyester: 358.03	[54]
45	Fe_3O_4-waste paper activated carbon composite (MB= 150 mg·L^{-1})	Pseudo-second order	0.999	–	–	5 h	55.86	[93]
46	Expired beverage (MB)	Pseudo-second order	0.996	–	–	40 min	408.22	[95]
47	Activated charcoal (AB and BB)	AB: Pseudo-second order BB: Pseudo-second order	AB: 0.99 BB: 0.99	–	–	1 h	–	[94]
48	Waste paper (MB and Cr(VI))	Pseudo-second order	H_2O_2 MB: 0.996 Cr(VI): 0.992 HNO_3 MB: 0.998 Cr(VI): 0.993 $KMnO_4$ MB: 0.997 Cr(VI): 0.994	–	H_2O_2 MB: 0.98 Cr(VI): 0.98 HNO_3 MB: 0.97 Cr(VI): 0.98 $KMnO_4$ MB: 0.98 Cr(VI): 0.98	MB: 1 h Cr(VI): 2 h	H_2O_2 MB: 30.16 Cr(VI): 29.10 HNO_3 MB: 34.11 Cr(VI): 35.52 $KMnO_4$ MB: 31.35 Cr(VI): 31.15	[96]
49	Date palm spikelets (MO =200 mg·L^{-1})	Non–linear Avrami	0.997	Stage 1: 0.969 Stage 2: 0.970 Stage 3: 0.997	–	4 h	200.93 (NSD: 6.11)	[97]

Notes: ECT: equilibrium contact time.

Those parameters can be a reference for spontaneous adsorption and type of adsorption. Moreover, analysis of intraparticle and film diffusions was not frequently conducted. Among the reviewed studies, only one reported the coefficient of determination (R^2) for each of the three stages of intraparticle diffusion. In addition, studies in the literature have not explained significantly different values of adsorption capacities in the experiment, isotherm equations, and kinetic equations. The adsorption capacities were still calculated using the Langmuir equation, despite being more compatible with Freundlich model. The use of three-parameter isotherm models is also rarely investigated.

The recovery and reusability of the adsorbent from activated carbons should be considered for future developments. Most studies did not measure these parameters, which influence the sustainability. Besides, the activated carbon must be usable in real wastewater containing dyes and/or heavy metals for industrial-scale application. Few studies have calculated root mean squared error (RMSE), normalized standard deviation (NSD), and average relative error (ARE%) for the adsorption isotherms, even though only one study analyzed the RMSE and ARE values of the kinetic curves. RMSE and ARE% are useful parameters to validate and measure the suitability of the experimental and prediction of adsorption capacities for the adsorption isotherms and kinetic models.

7. Conclusions

Increasing concern for environmental sustainability has led researchers to study the utilization of natural sources and waste as activated carbon-based adsorbent sources. The activation method governs activated carbons' physical conditions, yields, and performance in adsorbing water pollutants such as dyes and heavy metals. Testing system conditions also affect the optimal adsorption of each AC. Utilization of these adsorbents should not cause other problems for the environment. Thus, the recovery and reusability of the adsorbent from activated carbons must be considered for future developments. Activated carbon from expired beverages, peanut shells, bean dregs, *Camellia oleifera* seed shells, and coffee husks could be reused three, four, five, seven times, respectively, thus being more efficient. Besides, the activated carbon must be usable in real wastewater containing dyes or heavy metals for industrial-scale application. The papers overviewed in this work generally explored adsorption isotherms and adsorption kinetics from the interactions between activated carbons and water pollutants. Most activated carbons form protective monolayers, which obey the Langmuir and Freundlich adsorption isotherms. Other activated carbons are appropriate for Dubinin–Radushkevich, Redlich-Peterson, Sips, Toth, and Temkin adsorption isotherms. Adsorption, which follows the Freundlich isotherm, includes a heterogeneity factor (n or $1/n$). It relates to adsorption intensity. Meanwhile, several adsorptions from reviewed activated carbons that obey the Langmuir model were determined by the separation factor (R_L) to disclose its adsorption tendency. Based on thermodynamic parameter calculations (ΔG^{o}_{ads}), most of the adsorption processes of pollutants onto activated carbons are spontaneous with physical and chemical adsorption mechanism. Pseudo-second reaction order is the favored kinetic order for considerable AC in the reaction mechanism. However, only in a few studies the root mean squared error (RMSE), normalized standard deviation (NSD), and average relative error (ARE%) were calculated during the model validation.

Supplementary materials

No supplementary materials are available.

Data availability statement

Data sharing does not apply to this article as no new data were created or analyzed in this study.

Acknowledgments

None.

Author contributions

Conceptualization: M.J.B.
Data curation: M.J.B., L.R., and L.H.
Formal Analysis: M.J.B.
Funding acquisition: M.J.B.
Investigation: M.J.B.
Methodology: M.J.B.
Project administration: M.J.B.
Resources: M.J.B.
Software: M.J.B.
Supervision: M.J.B., L.R., and L.H.
Validation: M.J.B., L.R., and L.H.
Visualization: M.J.B.
Writing – original draft: M.J.B.
Writing – review & editing: M.J.B., L.R., and L.H.

Conflict of interest

The Author declares no conflict of interest

Additional information

Muhamad Jalil Baari: Researcher and Assistant Professor in the Department of Chemistry, Universitas Sembilanbelas November Kolaka. Scientific interest: Physical chemistry research, which focuses on material synthesis as corrosion and scale inhibitors, metal and dye adsorbent, biofuel, and waste treatment. Scopus ID 57215409862.

La Harimu: Researcher and Associate Professor in the Department of Chemistry Education, Universitas Halu Oleo, with expertise in Analytical Chemistry, particularly in membrane separation and Adsorption. In the field of membrane separation, La Harimu focuses on the separation of heavy metals. Meanwhile, research concerning adsorption focuses on the adsorption of heavy metals, colors, and oils. Scopus ID 57211795703.

La Rudi: Assistant Professor in the Department of Chemistry Education, Faculty of Teacher Training and Education, Universitas Halu Oleo, with expertise in Environmental Analytical Chemistry. His current research focuses on teaching methods and environmental analytical chemistry, particularly in coastal, island, and rural areas. Some of his studies include the adsorption of lead (Pb) ions from used oil using a combination of beach sand and rice husk charcoal as adsorbents, as well as the adsorption of metal ions using a combination of silica derived from nickel slag waste and chitosan extracted from shrimp shells. Scopus ID 57239702800.

8. References

1. Daneshvar N, Salari D, Khataee AR. Photocatalytic degradation of azo dye acid red 14 in water: Investigation of the effect of operational parameters. J Photochem Photobiol A Chem. 2003;157(1):111–116. doi:10.1016/S1010-6030(03)00015-7
2. Zhou Y, Lu J, Zhou Y, Liu Y. Recent advances for dyes removal using novel adsorbents: A review. Environ Pollut. 2019;252:352–365. doi:10.1016/j.envpol.2019.05.072
3. Haldorai Y, Kharismadewi D, Tuma D, Shim JJ. Properties of chitosan/magnetite nanoparticles composites for efficient dye adsorption and antibacterial agent. Korean J Chem Eng. 2015;32(8):1688–1693. doi:10.1007/s11814-014-0368-9
4. Vezentsev AI, Thuy DM, Goldovskaya-Peristaya LF, Glukhareva NA. Adsorption of methylene blue on the composite sorbent based on bentonite-like clay and hydroxyapatite. Indones J Chem. 2018;18(4):733–741. doi:10.22146/ijc.37050
5. Jasim AQ, Ajjam SK. Removal of heavy metal ions from wastewater using ion exchange resin in a batch process with kinetic isotherm. South African J Chem Eng. 2024;49:43–54. doi:10.1016/j.sajce.2024.04.002
6. Hassan MM, Carr CM. A critical review on recent advancements of the removal of reactive dyes from dyehouse effluent by ion-exchange adsorbents. Chemosphere. 2018;209:201–219. doi:10.1016/j.chemosphere.2018.06.043
7. Harimu L, Matsjeh S, Siswanta D, Santosa SJ, Baari MJ. Application of poly(ethyl eugenyl oxyacetate) compounds as the ions carrier for heavy metals separation and separation of Fe and Ni in ferronickel using liquid membrane transport method. Indones J Chem. 2022;22(4):1002–1013. doi:10.22146/ijc.72486
8. Sun Y, Zhou S, Pan SY, Zhu S, Yu Y, Zheng H. Performance evaluation and optimization of flocculation process for removing heavy metal. Chem Eng J. 2020;385:123911. doi:10.1016/j.cej.2019.123911
9. Utami M, Wang S, Musawwa MM, Purbaningtias TE, Fitri M, Yuspita I, Abd-Elkader OH, Yadav KK, Munusamy-Ramanujam G, Bang D, Chang SW, Ravindran B. Simultaneous photocatalytic removal of organic dye and heavy metal from textile wastewater over N-doped TiO_2 on reduced graphene oxide. Chemosphere. 2023;332:138882. doi:10.1016/j.chemosphere.2023.138882
10. Pathania D, Sharma S, Singh P. Removal of methylene blue by adsorption onto activated carbon developed from Ficus carica bast. Arab J Chem. 2017;10:S1445–S1451. doi:10.1016/j.arabjc.2013.04.021

11. Mittal A, Thakur V, Gajbe V. Adsorptive removal of toxic azo dye Amido Black 10B by hen feather. Environ Sci Pollut Res. 2013;20(1):260–269. doi:10.1007/s11356-012-0843-y
12. Martínez ML, Torres MM, Guzmán CA, Maestri DM. Preparation and characteristics of activated carbon from olive stones and walnut shells. Ind Crops Prod. 2006;23(1):23–28. doi:10.1016/j.indcrop.2005.03.001
13. Anshar AM, Taba P, Raya I. Kinetic and thermodynamics studies on the adsorption of phenol on activated carbon from rice husk activated by $ZnCl_2$. Indones J Sci Technol. 2016;1(1):47–60. doi:10.17509/ijost.v1i1.2213
14. Sudaryanto Y, Hartono SB, Irawaty W, Hindarso H, Ismadji S. High surface area activated carbon prepared from cassava peel by chemical activation. Bioresour Technol. 2006;97(5):734–739. doi:10.1016/j.biortech.2005.04.029
15. Zhou J, Luo A, Zhao Y. Preparation and characterisation of activated carbon from waste tea by physical activation using steam. J Air Waste Manag Assoc. 2018;68(12):1269–1277. doi:10.1080/10962247.2018.1460282
16. Pereira RG, Veloso CM, Da Silva NM, De Sousa LF, Bonomo RCF, De Souza AO, Da Guarda Souza MO, Da Costa Ilhéu Fontan R. Preparation of activated carbons from cocoa shells and siriguela seeds using H_3PO_4 and $ZnCl_2$ as activating agents for BSA and α-lactalbumin adsorption. Fuel Process Technol. 2014;126:476–486. doi:10.1016/j.fuproc.2014.06.001
17. Deng H, Yang L, Tao G, Dai J. Preparation and characterization of activated carbon from cotton stalk by microwave assisted chemical activation-Application in methylene blue adsorption from aqueous solution. J Hazard Mater. 2009;166(2–3):1514–1521. doi:10.1016/j.jhazmat.2008.12.080
18. Illingworth JM, Rand B, Williams PT. Non-woven fabric activated carbon produced from fibrous waste biomass for sulphur dioxide control. Process Saf Environ Prot. 2019;122:209–220. doi:10.1016/j.psep.2018.12.010
19. Corda NC, Kini MS. A Review on Adsorption of Cationic Dyes using Activated Carbon, MATEC Web Conf. 2018;144:02022. doi:10.1051/matecconf/201814402022
20. Czikkely M, Neubauer E, Fekete I, Ymeri P, Fogarassy C. Review of heavy metal adsorption processes by several organic matters from wastewaters. Water (Switzerland). 2018;10(10):1–15. doi:10.3390/w10101377
21. Arora R. Adsorption of Heavy Metals–A Review. Mater Today Proc. 2019;18:4745–4750. doi:10.1016/j.matpr.2019.07.462
22. Deliyanni EA, Kyzas GZ, Triantafyllidis KS, Matis KA. Activated carbons for the removal of heavy metal ions: A systematic review of recent literature focused on lead and arsenic ions. Open Chem. 2015;13(1):699–708. doi:10.1515/chem-2015-0087
23. Aprile A, De Bellis L. Editorial for special issue “heavy metals accumulation, toxicity, and detoxification in plants,”. Int J Mol Sci. 2020;21(11):1–5. doi:10.3390/ijms21114103
24. Hawkes SJ. What is a “Heavy Metal”?. J Chem Educ. 1997;74(11):1374. doi:10.1021/ed074p1374
25. Sureshkumar H. Removal of Heavy Metals from wastewater: A review. Ijaiem. 2015;4(10):19–22.
26. Kurniawan TA, Chan GYS, Lo WH, Babel S. Physico-chemical treatment techniques for wastewater laden with heavy metals. Chem Eng J. 2006;118(1–2):83–98. doi:10.1016/j.cej.2006.01.015
27. Aziz HA, Adlan MN, Ariffin KS. Heavy metals (Cd, Pb, Zn, Ni, Cu and Cr(III)) removal from water in Malaysia: Post treatment by high quality limestone. Bioresour Technol. 2008;99(6):1578–1583. doi:10.1016/j.biortech.2007.04.007
28. Hong YJ, Liao W, Yan ZF, Bai YC, Feng CL, Xu ZX, Xu DY. Progress in the Research of the toxicity effect mechanisms of heavy metals on freshwater organisms and their water quality criteria in China. J Chem. 2020;2020:1–12. doi:10.1155/2020/9010348
29. Theophanides T, Anastassopoulou J. Copper and carcinogenesis. Crit Rev Oncol Hematol. 2002;42(1):57–64. doi:10.1016/S1040-8428(02)00007-0
30. Dean JG, Bosqui FL, Lanouette KH. Removing heavy metals from wastewater. Environ Sci Technol. 1972;6(6):518–522. doi:10.1021/es60065a006
31. Qasem NAA, Mohammed RH, Lawal DU. Removal of heavy metal ions from wastewater: a comprehensive and critical review. NPJ Clean Water. 2021:4(1):36. doi:10.1038/s41545-021-00127-0
32. Ishmaturrahmi I, Rahmi R, Mustafa I. The influence of Fe_3O_4 on magnetic chitosan composite preparation for methylene blue removal from water. IOP Conf Ser Mater Sci Eng. 2019;523(1):4–11. doi:10.1088/1757-899X/523/1/012020
33. Rafatullah M, Sulaiman O, Hashim R, Ahmad A. Adsorption of methylene blue on low-cost adsorbents: A review. J Hazard Mater. 2010;177(1–3):70–80. doi:10.1016/j.jhazmat.2009.12.047
34. Altass HM, Morad M, Khder AERS, Mannaa MA, Jassas RS, Alsimaree AA, Ahmed SA, Salama RS. Enhanced catalytic activity for CO oxidation by highly active Pd nanoparticles supported on reduced graphene oxide /Copper metal organic framework. J Taiwan Inst Chem Eng. 2021;128:194–208. doi:10.1016/j.jtice.2021.08.034
35. Gupta VK, Suhas S. Application of low-cost adsorbents for dye removal – A review. J Environ Manage. 2009;90(8):2313–2342. doi:10.1016/j.jenvman.2008.11.017
36. Yagub MT, Sen TK, Afroze S, Ang HM. Dye and its removal from aqueous solution by adsorption: A review. Adv Colloid Interface Sci. 2014;209:174–182. doi:10.1016/j.cis.2014.04.002
37. Esvandi Z, Foroutan R, Peighambardoust SJ, Akbari A, Ramavandi B. Uptake of anionic and cationic dyes from water using natural clay and clay/starch/$MnFe_2O_4$ magnetic nanocomposite. Surfaces and Interfaces. 2020;21:100754. doi:10.1016/j.surfin.2020.100754
38. Wi E, Go S, Shin SY, Cheon HJ, Jeong G, Cheon H, Kim J, Jung HR, Kim H, Chang M. Highly efficient and selective removal of anionic dyes from aqueous solutions using magneto-responsive Fe-aminoclay/Fe_2O_3/polyvinyl alcohol composite microgels. Chem Eng J. 2023;454:140309. doi:10.1016/j.cej.2022.140309
39. Ngulube T, Gumbo JR, Masindi V, Maity A. An update on synthetic dyes adsorption onto clay based minerals: A state-of-art review. J Environ Manage. 2017;191:35–57. doi:10.1016/j.jenvman.2016.12.031
40. Ong ST, Lee CK, Zainal Z. Removal of basic and reactive dyes using ethylenediamine modified rice hull. Bioresour Technol. 2007;98(15):2792–2799. doi:10.1016/j.biortech.2006.05.011
41. Lin K, Zhao H. The Impact of Green finance on the ecologicalization of urban industrial structure—Based on GMM of dynamic panel system. J Artif Intell Technol. 2022;2:123–129. doi:10.37965/jait.2022.0115
42. Tan CHC, Sabar S, Hussin MH. Development of immobilized microcrystalline cellulose as an effective adsorbent for methylene blue dye removal. South African J Chem Eng. 2018;26:11–24. doi:10.1016/j.sajce.2018.08.001
43. Neolaka YAB, Riwu AAP, Aigbe UO, Ukhurebor KE, Onyancha RB, Darmokoesoemo H, Kusuma HS. Potential of activated carbon from various sources as a low-cost adsorbent to remove heavy metals and synthetic dyes. Results Chem. 2023;5:100711. doi:10.1016/j.rechem.2022.100711
44. Sun G, Xu X. Sunflower stalks as adsorbents for color removal from textile wastewater. Ind Eng Chem Res. 1997;36(3):808–812. doi:10.1021/ie9603833
45. Naidu AL, Sudarshan B, Krishna KH. Study on mechanical behavior of groundnut shell fiber reinforced polymer metal matrix composities. Int J Study Mech Behav Groundn Shell Fiber Reinf Polym Met Matrix Compos. 2013;2 Februari.
46. Cuhadaroglu D, Uygun OA. Production and characterization of activated carbon from a bituminous coal by chemical activation. African J Biotechnol. 2008;7(20):3706–3713.

47. Lillo-Ródenas MA, Lozano-Castelló D, Cazorla-Amorós D, Linares-Solano A. Preparation of activated carbons from Spanish anthracite: II. Activation by NaOH. Carbon N Y. 2001;39(5):751–759. doi:10.1016/S0008-6223(00)00186-X
48. Aldawsari A, Khan MA, Hameed BH, AlOthman ZA, Siddiqui, MR, Ahmed AYBH, Alsohaimi IH. Development of activated carbon from phoenix dactylifera fruit pits: Process optimization, characterization, and methylene blue adsorption. Desalin Water Treat. 2017;62:273–281. doi:10.5004/dwt.2017.0529
49. Sangon S, Hunt AJ, Attard TM, Mengchang P, Ngernyen Y, Supanchaiyamat N. Valorisation of waste rice straw for the production of highly effective carbon based adsorbents for dyes removal. J Clean Prod. 2018;172:1128–1139. doi:10.1016/j.jclepro.2017.10.210
50. Baysal M, Bilge K, Yılmaz B, Papila M, Yürüm Y. Preparation of high surface area activated carbon from waste-biomass of sunflower piths: Kinetics and equilibrium studies on the dye removal. J Environ Chem Eng. 2018;6(2):1702–1713. doi:10.1016/j.jece.2018.02.020
51. Yun CH, Park YH, Park CR. Effects of pre-carbonization on porosity development of activated carbons from rice straw. Carbon N Y. 2001;39(4):559–567. doi:10.1016/S0008-6223(00)00163-9
52. Sajjadi SA, Meknati A, Lima EC, Dotto GL, Mendoza-Castillo DI, Anastopoulos I, Alakhras F, Unuabonah EI, Singh P, Hosseini-Bandegharaei A. A novel route for preparation of chemically activated carbon from pistachio wood for highly efficient Pb(II) sorption. J Environ Manage. 2019;236:34–44. doi:10.1016/j.jenvman.2019.01.087
53. Ma R, Qin X, Liu Z, Fu Y. Adsorption property, kinetic and equilibrium studies of activated carbon fiber prepared from liquefied wood by $ZnCl_2$ activation. Materials (Basel). 2019;12(9):1377. doi:10.3390/ma12091377
54. Carraro PS, Spessato L, Crespo LHS, Yokoyama JTC, Fonseca JM, Bedin KC, Ronix A, Cazetta AL, Silva TL, Almeida VC. Activated carbon fibers prepared from cellulose and polyester–derived residues and their application on removal of Pb^{2+} ions from aqueous solution. J Mol Liq. 2019;289:111150. doi:10.1016/j.molliq.2019.111150
55. Budarin V, Clark J, Deswarte F, Hardy J, Hunt A, Kerton F. Delicious not siliceous: Expanded carbohydrates as renewable separation media for column chromatography. Chem Commun (Camb). 2005;23:2903–2905. doi:10.1039/b502330k
56. Butcher DJ. The Essence of Chromatography By Colin F. Poole. J Am Chem Soc. 2003;125(33):10144–10145. doi:10.1021/ja033507t
57. Muslim A, Ellysa E, Said SD. Cu(II) ion adsorption using activated carbon prepared from pithecellobium jiringa (Jengkol) shells with ultrasonic assistance: isotherm, kinetic and thermodynamic studies. J Eng Technol Sci. 2017;49(4):472–490. doi:10.5614/j.eng.technol.sci.2017.49.4.4
58. Islam MA, Sabar S, Benhouria A, Khanday WA, Asif M, Hameed BH. Nanoporous activated carbon prepared from karanj (Pongamia pinnata) fruit hulls for methylene blue adsorption. J Taiwan Inst Chem Eng. 2017;74:96–104. doi:10.1016/j.jtice.2017.01.016
59. Alcaraz L, Fernández AL, García-Díaz I, López FA. Preparation and characterization of activated carbons from winemaking wastes and their adsorption of methylene blue. Adsorpt Sci Technol. 2018;36(5–6):1331–1351. doi:10.1177/0263617418770295
60. Centeno TA, Stoeckli F. The assessment of surface areas in porous carbons by two model-independent techniques, the DR equation and DFT. Carbon N Y. 2010;48(9):2478–2486. doi:10.1016/j.carbon.2010.03.020
61. Khuluk RH, Rahmat A, Buhani B, Suharso S. Removal of Methylene blue by adsorption onto activated carbon from coconut shell (Cocous Nucifera L.). Indones J Sci Technol. 2019;4(2):229–240. doi:10.17509/ijost.v4i2.18179
62. El Jery A, Alawamleh HSK, Sami MH, Abbas HA, Sammen SS, Ahsan A, Imteaz MA, Shanableh A, Shafiquzzaman M, Osman H, Al-Ansari N. Isotherms, kinetics and thermodynamic mechanism of methylene blue dye adsorption on synthesized activated carbon. Sci Rep. 2024;14(1):1–12. doi:10.1038/s41598-023-50937-0
63. Jawad AH, Abdulhameed AS, Wilson LD, Syed-Hassan SSA, ALOthman ZA, Khan MR. High surface area and mesoporous activated carbon from KOH-activated dragon fruit peels for methylene blue dye adsorption: Optimization and mechanism study. Chinese J Chem Eng. 2021;32:281–290. doi:10.1016/j.cjche.2020.09.070
64. Jawad AH, Abdulhameed AS. Statistical modeling of methylene blue dye adsorption by high surface area mesoporous activated carbon from bamboo chip using KOH-assisted thermal activation. Energy Ecol Environ. 2020;5(6):456–469. doi:10.1007/s40974-020-00177-z
65. El Maguana Y, Elhadiri N, Benchanaa M, Chikri R. Activated carbon for dyes removal: modeling and understanding the adsorption process. J Chem. 2020;2020:1–9. doi:10.1155/2020/2096834
66. Maguana Y. El Elhadiri N, Bouchdoug M, Benchanaa M, Jaouad A. Activated carbon from prickly pear seed cake : Optimization of preparation conditions using experimental design and its application in dye removal. Int J Chem Engineer. 2019;2019:1–12. doi:10.1155/2019/8621951
67. El Maguana Y. Elhadiri N, Benchanaa M, Chikri R. Adsorption thermodynamic and kinetic studies of methyl orange onto sugar scum powder as a low-cost inorganic adsorbent. J Chem. 2020;2020:1–10. doi:10.1155/2020/9165874
68. Kheddo A, Rhyman L, Elzagheid MI, Jeetah P, Ramasami P. Adsorption of synthetic dyed wastewater using activated carbon from rice husk. SN Appl Sci. 2020;2(12):1–14. doi:10.1007/s42452-020-03922-5
69. Mopoung S, Dejang N. Activated carbon preparation from eucalyptus wood chips using continuous carbonization–steam activation process in a batch intermittent rotary kiln. Sci Rep. 2021;11(1):1–9. doi:10.1038/s41598-021-93249-x
70. Pagalan E, Sebron M, Gomez S, Salva SJ, Ampusta R, Macarayo AJ, Joyno C, Ido A, Arazo R. Activated carbon from spent coffee grounds as an adsorbent for treatment of water contaminated by aniline yellow dye. Ind Crops Prod. 2020;145(June):111953. doi:10.1016/j.indcrop.2019.111953
71. Wang D, Wang Z, Zheng X, Tian M. Activated carbon fiber derived from the seed hair fibers of Metaplexis japonica: Novel efficient adsorbent for methylene blue. Ind Crops Prod. 2020;148:112319. doi:10.1016/j.indcrop.2020.112319
72. Guo H, Bi C, Zeng C, Ma W, Yan L, Li K, Wei K. Camellia oleifera seed shell carbon as an efficient renewable bio-adsorbent for the adsorption removal of hexavalent chromium and methylene blue from aqueous solution. J Mol Liq. 2018;249:629–636. doi:10.1016/j.molliq.2017.11.096
73. Hashem HM, El-Maghrabey M, El-Shaheny R. Inclusive study of peanut shells derived activated carbon as an adsorbent for removal of lead and methylene blue from water. Sci Rep. 2024;14(1):1–24. doi:10.1038/s41598-024-63585-9
74. Samiyammal P, Kokila A, Pragasan LA, Rajagopal R, Sathya R, Ragupathy S, Krishnakumar M, Reddy VRM. Adsorption of brilliant green dye onto activated carbon prepared from cashew nut shell by KOH activation: Studies on equilibrium isotherm. Environ Res. 2022;212(PD):113497. doi:10.1016/j.envres.2022.113497
75. Deivasigamani P, Kumar PS, Sundaraman S, Soosai MR, Renita AA, Karthikeyan M, Bektenov N, Baigenzhenov O, Venkatesan D, Kumar JA. Deep insights into kinetics, optimization and thermodynamic estimates of methylene blue adsorption from aqueous solution onto coffee husk (Coffee arabica) activated carbon. Environ Res. 2023;236:116735. doi:10.1016/j.envres.2023.116735
76. Yaqub A, Syed SM, Ajab H, Zia Ul Haq M. Activated carbon derived from Dodonaea Viscosa into beads of calcium-alginate for the sorption of methylene blue (MB): Kinetics,

equilibrium and thermodynamics. J Environ Manage. 2023;327:116925. doi:10.1016/j.jenvman.2022.116925

77. Alkhabbas M, Al-Ma'abreh AM, Edris G, Saleh T, Alhmood H. Adsorption of anionic and cationic dyes on activated carbon prepared from oak cupules: Kinetics and Thermodynamics studies. Int J Environ Res Public Health. 2023;20(4):3280. doi:10.3390/ijerph20043280
78. Van Thuan T, Quynh BTP, Nguyen TD, Ho VTT, Bach LG. Response surface methodology approach for optimization of Cu^{2+}, Ni^{2+}, and Pb^{2+} adsorption using KOH-activated carbon from banana peel. Surfaces and Interfaces. 2017;6:209–217. doi:10.1016/j.surfin.2016.10.007
79. Muslim A. Australian Pine Cones-Based Activated Carbon for Adsorption of Copper in Aqueous Solution. J Eng Sci Technol. 2017;12(2):280–295.
80. Enniya I, Rghioui L, Jourani A. Adsorption of hexavalent chromium in aqueous solution on activated carbon prepared from apple peels. Sustain Chem Pharm. 2018;7(December 2017):9–16. doi:10.1016/j.scp.2017.11.003
81. Chu B, Amano Y, Machida M. Preparation of bean dreg derived N-doped activated carbon with high adsorption for Cr(VI). Colloids Surfaces A Physicochem Eng Asp. 2020;586(VI):124262. doi:10.1016/j.colsurfa.2019.124262
82. Kharrazi SM, Mirghaffari N, Dastgerdi MM, Soleimani M. A novel post-modification of powdered activated carbon prepared from lignocellulosic waste through thermal tension treatment to enhance the porosity and heavy metals adsorption. Powder Technol. 2020;366:358–368. doi:10.1016/j.powtec.2020.01.065
83. Changmai M, Banerjee P, Nahar K, Purkait MK. A novel adsorbent from carrot, tomato and polyethylene terephthalate waste as a potential adsorbent for Co(II) from aqueous solution: Kinetic and equilibrium studies. J Environ Chem Eng. 2018;6(1):246–257. doi:10.1016/j.jece.2017.12.009
84. Boeykens SP, Redondo N, Obeso RA, Caracciolo N, Vázquez C. Chromium and Lead adsorption by avocado seed biomass study through the use of total Reflection X-Ray fluorescence analysis. Appl Radiat Isot. 2019;153(June):108809. doi:10.1016/j.apradiso.2019.108809
85. Karim MA, Yuniar H, Lestari CC, Widowati TW. Removal of heavy metals from textile wastewater using a mixture of carbon from bare hands and carbide waste as an adsorbent. J Ecol Eng. 2024;25(1):245–255. doi:10.12911/22998993/175248
86. Touzani I, El Machrafi I, Harboul K, Boudouch O, Alouiz I, Hammani K, Flouchi R, Fikri-Benbrahim K. Evaluation of activated carbons prepared from bioprecursors for the removal of cadmium and chromium (VI). Appl Environ Soil Sci. 2024;2024:1–11. doi:10.1155/2024/8663114
87. Ishar I, Taba P, Fahruddin F. Effectiveness of activated carbon from nutmeg shell (Myristica fragrans) waste as adsorbent for metal ions Pb(II) and Cu(II) in liquid waste. Nat Environ Pollut Technol. 2024;23(2):1075–1083. doi:10.46488/nept.2024.v23i02.041
88. Sukmono Y, Kristanti RA, Foo BV, Hadibarata T. Adsorption of Fe and Pb from aqueous solution using coconut shell activated carbon. Biointerface Res Appl Chem. 2024;14(2):1–14. doi:10.33263/BRIAC142.030
89. Al-Ma'Abreh AM, Hmedat DA, Edris G, Hamed MA. Removal of heavy metal ions (Pb^{2+}, Co^{2+}, and Cd^{2+}) by Activated carbon from cypress fruit: an investigation of kinetics, thermodynamics, and isotherms. J Chem. 2024;2024:1–13. doi:10.1155/2024/1984821
90. Osasona I, Aiyedatiwa K, Johnson JA, Faboya OL. Activated carbon from spent brewery barley husks for cadmium ion adsorption from aqueous solution. Indones J Chem. 2018;18(1):145–152. doi:10.22146/ijc.22422
91. Hassan AF, Elhadidy H. Production of activated carbons from waste carpets and its application in methylene blue adsorption: Kinetic and thermodynamic studies. J Environ Chem Eng. 2017;5(1):955–963. doi:10.1016/j.jece.2017.01.003
92. Nhi NTT, Tho NTM, Anh NTH. An efficient adsorbent for the removal of dyes prepared by an in situ growth of ZIF-8 onto activated carbon. Green Chem Lett Rev. 2024;17(1):1–16. doi:10.1080/17518253.2024.2377555
93. Fisli A, Safitri RD, Nurhasni N, Dewi SH, Deswita D. Isotherm, kinetics, and thermodynamics adsorption studies of dye onto Fe$_3$O$_4$-waste paper activated carbon composites. J Teknologi. 2021;83(1):45–55. doi:10.11113/jurnalteknologi.v83.14991
94. Ali F, Ali N, Bibi I, Said A, Nawaz S, Ali Z, Salman SM, Iqbal HMN, Bilal M. Adsorption isotherm, kinetics and thermodynamic of acid blue and basic blue dyes onto activated charcoal. Case Stud Chem Environ Eng. 2020;2(September):100040. doi:10.1016/j.cscee.2020.100040
95. Liu Y, Huo Z, Song Z, Zhang C, Ren D, Zhong H, Jin F. Preparing a magnetic activated carbon with expired beverage as carbon source and KOH as activator. J Taiwan Inst Chem Eng. 2019;96:575–587. doi:10.1016/j.jtice.2018.11.017
96. Mabalane K, Thabede PM, Shooto ND. Activated carbon from paper waste as potential adsorbents for methylene blue and hexavalent chromium. Appl Sci. 2024;14(11):4585. doi:10.3390/app14114585
97. Al-Hazeef MSF, Aidi A, Hecini L, Osman AI, Hasan GG, Al-thamthami M, Ziad S, Otmane T, Rooney DW. Valorizing date palm spikelets into activated carbon-derived composite for methyl orange adsorption: advancing circular bioeconomy in wastewater treatment—a comprehensive study on its equilibrium, kinetics, thermodynamics, and mechanisms. Environ Sci Pollut Res. 2024;31(38):50493–50512. doi:10.1007/s11356-024-34581-3
98. Tsai WC, de Luna MDG, Bermillo-Arriesgado HLP, Futalan CM, Colades JI, Wan MW. Competitive fixed-bed adsorption of Pb(II), Cu(II), and Ni(II) from aqueous solution using chitosan-coated bentonite. Int J Polym Sci. 2016;2016(1):1608939. doi:10.1155/2016/1608939
99. Abdulhameed A, AbdulKarim-Talaq M, Jawad AH. Modeling and mechanism of reactive orange 16 dye adsorption by chitosan-glyoxal/ TiO$_2$ nanocomposite: application of response surface methodology. Desalin water Treat. 2019;164:346–360. doi:10.1155/2016/1608939
100. Safa Y, Bhatti HN. Kinetic and thermodynamic modeling for the removal of Direct Red-31 and Direct Orange-26 dyes from aqueous solutions by rice husk. Desalin. 2011;272(1):313–322. doi:10.1016/j.desal.2011.01.040
101. Foo KY, Hameed BH. Insights into the modeling of adsorption isotherm systems. Chem Eng J. 2010;156(1):2–10. doi:10.1016/j.cej.2009.09.013
102. Pezoti O, Cazetta AL, Souza IPAF, Bedin KC, Martins AC, Silva TL, Almeida VC. Adsorption studies of methylene blue onto ZnCl$_2$-activated carbon produced from buriti shells (Mauritia flexuosa L.). J Ind Eng Chem. 2014;20(6):4401–4407. doi:10.1016/j.jiec.2014.02.007
103. Benmessaoud A, Nibou D, Mekatel EH, Amokrane S. A comparative study of the linear and non-linear methods for determination of the optimum equilibrium isotherm for adsorption of Pb^{2+} ions onto Algerian treated clay. Iran J Chem Chem Eng. 2020;39(4):153–171. doi:10.1016/j.jiec.2014.02.007
104. Huang CH, Chang KP, Ou HD, Chiang YC, Wang CF. Adsorption of cationic dyes onto mesoporous silica. Microporous Mesoporous Mater. 2011;141(1).102–109. doi:10.1016/j.micromeso.2010.11.002
105. Mittal H, Ray SS. A study on the adsorption of methylene blue onto gum ghatti/TiO$_2$ nanoparticles-based hydrogel nanocomposite. Int J Biol Macromol. 2016;88:66–80. doi:10.1016/j.micromeso.2010.11.002
106. Gao JJ, Qin YB, Zhou T, Cao DD, Xu P, Hochstetter D, Wang YF. Adsorption of methylene blue onto activated carbon produced from tea (Camellia sinensis L.) seed shells: kinetics, equilibrium, and thermodynamics studies. J

Zhejiang Univ Sci B. 2013;14(7):650–658. doi:10.1631/jzus.B12a0225
107. Tran HN, You SJ, Chao HP. Thermodynamic parameters of cadmium adsorption onto orange peel calculated from various methods: A comparison study. J Environ Chem Eng. 2016;4(3):26712–682. doi:10.1016/j.jece.2016.05.009
108. Kumar KV, Sivanesan S. Prediction of optimum sorption isotherm: Comparison of linear and non-linear method. J Hazard Mater. 2005;126(1):198–201. doi:10.1016/j.jhazmat.2005.06.007
109. Parimal S, Prasad M, Bhaskar U. Prediction of Equilibrium Sorption Isotherm: Comparison of Linear and Nonlinear Methods. Ind Eng Chem Res. 2010;49(6):2882–2888. doi:10.1021/ie9013343
110. Langmuir I. The adsorption of gases on plane surfaces of glass, mica and platinum. J Am Chem Soc. 1918;40(9):1361–1403. doi:10.1021/ja02242a004
111. McKay G. Use of adsorbents for the removal of pollutants from wastewaters. Boca Raton: CRC Press;1995.FL SE- 86 p: illustrations.
112. Vitek R, Masini JC. Nonlinear regression for treating adsorption isotherm data to characterize new sorbents: Advantages over linearization demonstrated with simulated and experimental data. Heliyon. 2023;9(4):e15128. doi:10.1016/j.heliyon.2023.e15128
113. Jong ST, Yoo CY, Kiew PL. Feasibility study of methylene blue adsorption using magnetized papaya seeds. Prog Energy Environ. 2020;14(1):1–12.
114. Serafin J, Dziejarski B. Application of isotherms models and error functions in activated carbon CO_2 sorption processes. Microporous Mesoporous Mater. 2023;354(January):112513. doi:10.1016/j.micromeso.2023.112513
115. Prasad RK, Srivastava SN. Sorption of distillery spent wash onto fly ash: Kinetics and mass transfer studies. Chem Eng J. 2009;146(1):90–97. doi:10.1016/j.cej.2008.05.021
116. Günay A, Arslankaya E, Tosun İ. Lead removal from aqueous solution by natural and pretreated clinoptilolite: Adsorption equilibrium and kinetics. J Hazard Mater. 2007;146(1):362–371. doi:10.1016/j.jhazmat.2006.12.034
117. Tóth J. Calculation of the BET-compatible surface area from any type I isotherms measured above the critical temperature. J Colloid Interface Sci. 2000;225(2):378–383. doi:10.1006/jcis.2000.6723
118. Buhani B, Narsito N, Nuryono N, Kunarti ES, Suharso S.. Adsorption competition of Cu(II) ion in ionic pair and multi-metal solution by ionic imprinted amino-silica hybrid adsorbent, Desalin Water Treat. 2015;55(5):1240–1252. doi:10.1080/19443994.2014.924880
119. Ahmad A, Rafatullah M, Sulaiman O, Ibrahim MH, Chii YY, Siddique BM. Removal of Cu(II) and Pb(II) ions from aqueous solutions by adsorption on sawdust of Meranti wood. Desalin. 2009;247(1):636–646. doi:10.1016/j.desal.2009.01.007
120. Chen D, Chen J, Luan X, Ji H, Xia Z. Characterization of anion-cationic surfactants modified montmorillonite and its application for the removal of methyl orange. Chem Eng J. 2011;171(3):1150–1158. doi:10.1016/j.cej.2011.05.013
121. Khamirchi R, Hosseini-Bandegharaei A, Alahabadi A, Sivamani S, Rahmani-Sani A, Shahryari T, Anastopoulos I, Miri M, Tran HN. Adsorption property of Br-PADAP-impregnated multiwall carbon nanotubes towards uranium and its performance in the selective separation and determination of uranium in different environmental samples. Ecotoxicol Environ Saf. 2018;150:136–143. doi:10.1016/j.ecoenv.2017.12.039
122. Li L, Liu F, Duan H, Wang X, Li J, Wang Y, Luo C. The preparation of novel adsorbent materials with efficient adsorption performance for both chromium and methylene blue. Colloids Surface B Biointerface. 2016;141:253–259. doi:10.1016/j.colsurfb.2015.06.023
123. Azizian S, Eris S, Wilson LD. Re-evaluation of the century-old Langmuir isotherm for modeling adsorption phenomena in solution. Chem Phys. 2018;513:99–104. doi:10.1016/j.chemphys.2018.06.022
124. Baseri JR, Palanisamy PN, Siva Kumar P. Adsorption of basic dyes from synthetic textile effluent by activated carbon prepared from Thevetia peruviana. Indian J Chem Technol. 2012;19(5):311–321.
125. Ho YS, McKay G. Pseudo-second order model for sorption processes. Process Biochem. 1999;34(5):451–465. doi:10.1016/j.jhazmat.2005.12.043
126. Aroua MK, Leong SPP, Teo LY, Yin CY, Daud WMAW. Real-time determination of kinetics of adsorption of lead(II) onto palm shell-based activated carbon using ion selective electrode. Bioresour Technol. 2008;99(13):5786–5792. doi:10.1016/j.biortech.2007.10.010
127. Benjelloun M, Miyah Y, Akdemir Evrendilek G, Zerrouq F, Lairini S. Recent advances in adsorption kinetic models: their application to dye types, Arab J Chem. 2021;14(4):103031. doi:10.1016/j.arabjc.2021.103031
128. Ho YS. Review of second-order models for adsorption systems, J Hazard Mater. 2006;136(3):681–689. doi:10.1016/j.jhazmat.2005.12.043
129. Islam MA, Benhouria A, Asif M, Hameed BH. Methylene blue adsorption on factory-rejected tea activated carbon prepared by conjunction of hydrothermal carbonization and sodium hydroxide activation processes. J Taiwan Inst Chem Eng. 2015;52:57–64. doi:10.1016/j.jtice.2015.02.010
130. Zhang X, Lv L, Qin Y, Xu M, Jia X, Chen Z. Removal of aqueous Cr(VI) by a magnetic biochar derived from Melia azedarach wood. Bioresour Technol. 2018;256:1–10. doi:10.1016/j.biortech.2018.01.145
131. Njoku VO, Islam MA, Asif M, Hameed BH. Preparation of mesoporous activated carbon from coconut frond for the adsorption of carbofuran insecticide. J Anal Appl Pyrolysis. 2014;110:172–180. doi:10.1016/j.jaap.2014.08.020